Lunar precursor effects in the solar wind and terrestrial magnetosphere

J. S. Halekas,[1,2] A. R. Poppe,[1,2] W. M. Farrell,[2,3] G. T. Delory,[1,2] V. Angelopoulos,[4] J. P. McFadden,[1] J. W. Bonnell,[1] K. H. Glassmeier,[5] F. Plaschke,[4] A. Roux,[6] and R. E. Ergun[7]

Received 25 October 2011; revised 14 March 2012; accepted 21 March 2012; published 2 May 2012.

[1] The two ARTEMIS probes observe significant precursor activity upstream from the Moon, when magnetically connected to the dayside lunar surface. The most common signature consists of high levels of whistler wave activity near half of the electron cyclotron frequency. This precursor activity extends to distances of many thousands of km, in both the solar wind and terrestrial magnetosphere. In the magnetosphere, electrons reflect from a combination of magnetic and electrostatic fields above the lunar surface, forming loss cone distributions. In the solar wind they generally form conics, as a result of reflection from an obstacle moving with respect to the plasma frame (just as at a shock). The anisotropy associated with these reflected electrons provides the free energy source for the whistlers, with cyclotron resonance conditions met between the reflected source population and Moonward-propagating waves. These waves can in turn affect incoming plasma, and we observe significant perpendicular electron heating and plasma density depletions in some cases. In the magnetosphere, we also observe broadband electrostatic modes driven by beams of secondary electrons and/or photoelectrons accelerated outward from the surface. We also occasionally see waves near the ion cyclotron frequency in the magnetosphere. These lower frequency waves, which may result from the presence of ions of lunar origin, modulate the whistlers described above, as well as the electrons. Taken together, our observations suggest that the presence of the Moon leads to the formation of an upstream region analogous in many ways to the terrestrial electron foreshock.

Citation: Halekas, J. S., et al. (2012), Lunar precursor effects in the solar wind and terrestrial magnetosphere, *J. Geophys. Res.*, *117*, A05101, doi:10.1029/2011JA017289.

1. Introduction

[2] The interaction of solar wind and magnetospheric plasma with the Moon and its exosphere, surface, and crustal magnetic fields generates a number of interesting plasma effects. These include the formation of a plasma wake, electrostatic charging of the surface, and ion and electron reflection by surface scattering, magnetic mirroring, and electrostatic forces. As reviewed by *Halekas et al.* [2011b], many of these processes have an essentially kinetic nature. The lunar environment provides a fascinating location to study fundamental plasma processes.

[3] The typical view of the lunar plasma interaction consists of plasma absorption at the upstream surface, and formation of a plasma wake downstream from the Moon, with few effects expected upstream from the surface except perhaps in regions of strong crustal magnetic fields. Recent observations have begun to change this view. We now know that a large fraction of solar wind hydrogen reflects from the surface, most in neutral form [*McComas et al.*, 2009; *Wieser et al.*, 2009], but a small percentage as ions [*Saito et al.*, 2008]. Above regions of strong crustal fields, up to 50% of the incident solar wind protons reflect [*Lue et al.*, 2011; *Saito et al.*, 2012], as do even larger fractions of electrons approaching 100% [*Anderson et al.*, 1975; *Halekas et al.*, 2001; *Mitchell et al.*, 2008]. In addition, ionized exospheric constituents [*Stern*, 1999] and sputtered ions from the surface [*Yokota et al.*, 2009] exist around the Moon, as do secondary electrons and photoelectrons,

[1]Space Sciences Laboratory, University of California, Berkeley, California, USA.
[2]Lunar Science Institute, NASA Ames Research Center, Moffett Field, California, USA.
[3]NASA Goddard Space Flight Center, Greenbelt, Maryland, USA.
[4]Department of Earth and Space Sciences, University of California, Los Angeles, California, USA.
[5]Institut für Geophysik und Extraterrestrische Physik, Technische Universität Braunschweig, Braunschweig, Germany.
[6]Laboratoire de Physique des Plasmas, Paris, France.
[7]Laboratory for Atmospheric and Space Physics, University of Colorado Boulder, Boulder, Colorado, USA.

Corresponding Author: J. S. Halekas, Space Sciences Laboratory, University of California, 7 Gauss Way, Berkeley, CA 94720, USA. (jazzman@ssl.berkeley.edu)

0148-0227/12/2011JA017289

which can be accelerated from the surface to form beams [*Halekas et al.*, 2008b]. All of these charged particle populations may affect the incoming plasma.

[4] In fact, a number of indications point to the significant effects of reflected and surface-generated particle populations on the ambient plasma. *Halekas et al.* [2012] found suggestions that magnetically reflected electrons may perturb the incoming solar wind halo/strahl electron distribution, probably through wave-particle effects. Numerous waves indisputably exist upstream from the Moon, especially on magnetic field lines connected to its surface, including low frequency (0.1–10 Hz) monochromatic [*Lin et al.*, 1998; *Halekas et al.*, 2006; *Tsugawa et al.*, 2011] and broadband [*Nakagawa et al.*, 2009; *Halekas et al.*, 2008a] electromagnetic waves, and higher frequency (10s of KHz) electrostatic waves [*Bale et al.*, 1997]. Some waves, including low frequency whistlers [*Farrell et al.*, 1996; *Nakagawa et al.*, 2003] also originate in the wake. Recently, *Santolík et al.* [2011] found similar indications of similar wave precursor activity at Rhea, and these same processes likely operate at many other airless bodies in the solar system.

[5] The ARTEMIS mission [*Angelopoulos*, 2012] provides the most comprehensive plasma and wave measurements yet from a dedicated lunar mission, and its two-probe capability allows separation of lunar phenomena from other confounding effects (for example, convected solar wind instabilities and terrestrial foreshock effects). In this paper, we discuss ARTEMIS observations of a variety of lunar precursor effects, several not previously reported. In the solar wind, many of these precursor effects have clear analogies to terrestrial electron foreshock phenomena. In the terrestrial magnetotail, despite the very different plasma environment, many of the same precursor effects occur, enabling comparisons of the effects of different inputs.

2. Lunar Precursor Observations in the Solar Wind

2.1. Overview of Solar Wind Observations

[6] We first discuss an ARTEMIS P1 lunar flyby in the solar wind, on August 6th, 2011. We have observed similar precursor effects on many orbits, but this case has some particularly interesting characteristics, as well as a long period of burst data (the highest time resolution observations available). We show an overview of the flyby in Figure 1, with observations from the ESA (ElectroStatic Analyzer) [*McFadden et al.*, 2008], EFI (Electric Field Instrument) [*Bonnell et al.*, 2008], SCM (Search Coil Magnetometer) [*Roux et al.*, 2008], and FGM (Fluxgate Magnetometer) [*Auster et al.*, 2008] instruments.

[7] During this flyby, the Moon's orbit placed ARTEMIS P1 in the solar wind, at average GSE coordinates of [3, 58, −3] earth radii, well outside of the terrestrial magnetosphere. For the most part, the incident plasma population appears to have the characteristics of the undisturbed solar wind. Given the spacecraft location to the side of the magnetosphere, and the large prevailing By component, the positive Bx observed during most of the interval ensures no magnetic connection between the Moon and the terrestrial bow shock (i.e., the Moon is not in the electron foreshock for most of the time period). However, when Bx decreases, changing the magnetic field geometry and plausibly placing the spacecraft in the Earth's foreshock, several events of note, most likely related to the foreshock, impact the lunar environment. We see strongly field aligned Moonward-going bursts of electrons at 5:43:30–5:44:30, 5:50–5:50:30, and 5:52–5:58. These bursts, especially the third, show the velocity dispersion characteristic of Type II events generated at an interplanetary shock or the terrestrial foreshock [*Fitzenreiter et al.*, 1996; *Bale et al.*, 1999]. Each burst takes place at the same time as a decrease in Bx, implying likely magnetic connection to the terrestrial foreshock. The velocity-dispersed electrons travel anti-parallel to the magnetic field, from the terrestrial foreshock toward the Moon. These disturbances provide interesting test cases of varying plasma inputs to the Moon for this event.

[8] The solar wind ions in Figure 1a show no clear effects of any of the disturbances mentioned above, nor of the presence of the Moon nearby. The electrons coming from the direction of the Moon (Figure 1c, outward-traveling, parallel to the magnetic field), however, have highly disturbed characteristics on flux tubes connected to the surface (as inferred by a straight line magnetic field trace from the spacecraft). The spectra of these outward-going electrons show a dropout in flux at energies above a few hundred eV during every interval of magnetic connection (even very short intervals such as the one at ∼05:38:30), and rapidly varying "bursty" characteristics at energies below ∼100 eV during these connected intervals. The flux dropout at high energies results from the blockage of that portion of the electron distribution by the solid obstacle. The low energy flux, on the other hand, must correspond to electrons either reflected from or produced near the lunar surface.

[9] Intriguingly, we see a signature that looks like velocity dispersion in the outward-going electrons in Figure 1c at energies below a few hundred eV, extending from the start of the connected interval at ∼5:40 to ∼5:42. True velocity dispersion cannot explain the duration of the feature, given the short expected travel time (a few seconds) from the Moon to the spacecraft for electrons of even a few eV. In fact, this signature most likely results from the very large deHoffman-Teller frame transformation velocities [*deHoffman and Teller*, 1950] near the point where the magnetic field meets the lunar surface at a tangent.

[10] We show a schematic figure of the flyby geometry in Figure 2. We can most easily understand electron reflection from a moving obstacle such as the Moon (or more precisely, from the combination of magnetic and electric fields near the Moon) in the deHoffman-Teller frame, which has a transformation velocity relative to the solar wind frame of $-\mathbf{V_{sw}} \cdot \mathbf{n}/((\mathbf{B}/B) \cdot \mathbf{n})$ aligned with the IMF direction, where $\mathbf{V_{sw}}$ is the solar wind velocity, $\mathbf{B}$ is the magnetic field vector (and B the magnitude), and $\mathbf{n}$ is the obstacle unit normal vector. This frame transformation produces a reference frame in which no convection electric field exists, allowing easy analysis of electron reflection from an obstacle, assuming adiabatic behavior. Note that at the first point of magnetic connection near the sub-solar point around ∼5:40, the frame transformation velocity will reach very large values, given nearly parallel velocity and surface normal, and nearly tangential incidence of the magnetic field at the surface. Electrons reflecting near this tangent point will therefore gain a large boost in velocity from drifts occurring during the reflection process. Electrons

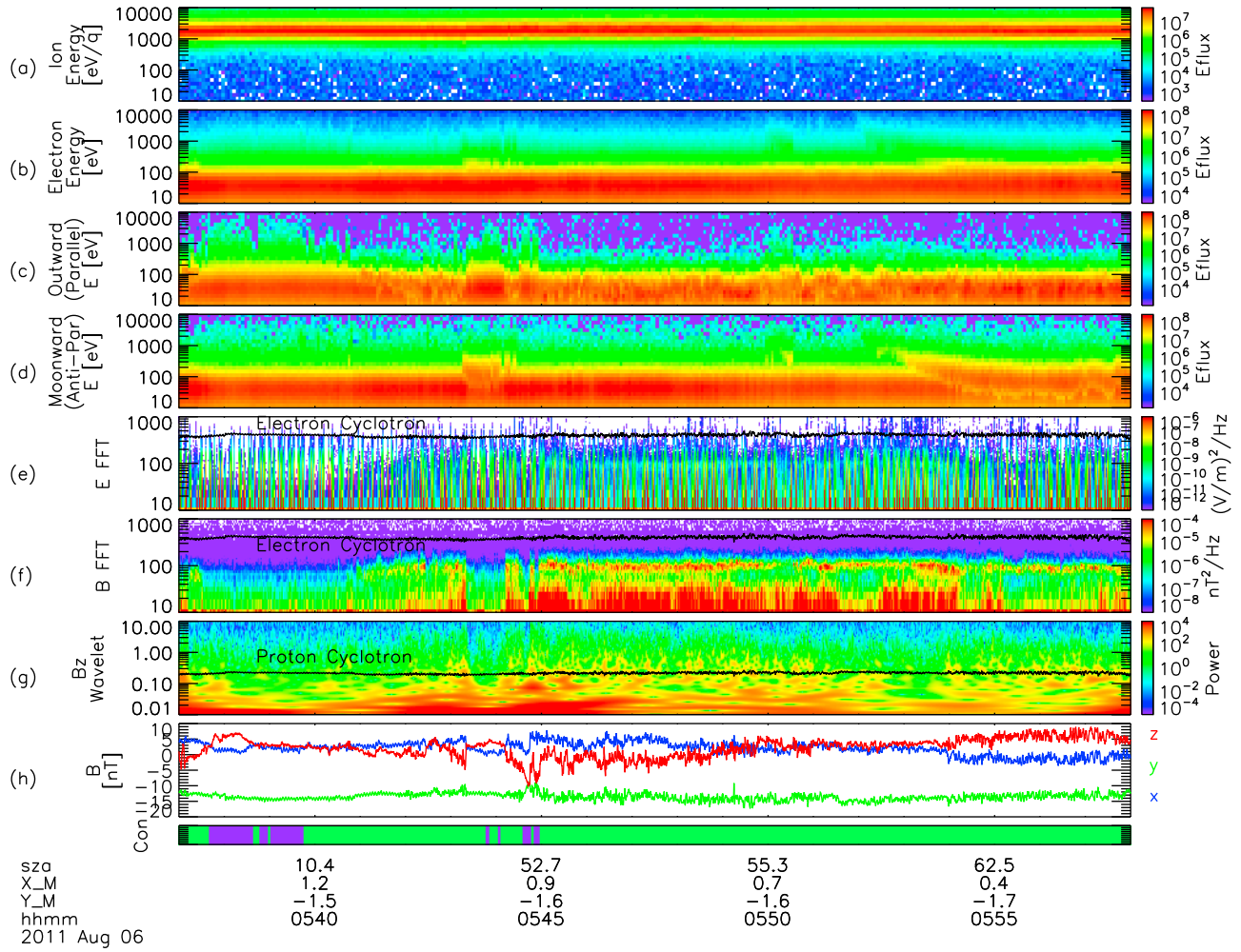

Figure 1. Data from an ARTEMIS P1 lunar flyby in the solar wind on August 6th, 2011. Omnidirectional differential energy flux spectra (eV/[eV cm^2 sr s]) for (a) ions and (b) electrons, spectra for electrons with pitch angles of (c) 0–15° (sunward/outward) and (d) 165–180° (Moonward), FFT wave spectra of high frequency (e) electric and (f) magnetic field, (g) wavelet spectra of low frequency magnetic field, and (h) magnetic field in SSE coordinates. Color bar indicates magnetic connection to the lunar surface in green or the wake in red (with periods with no connection to wake or surface in dark blue/purple). Text labels indicate surface solar zenith angle (SZA) when connected, spacecraft (X, Y) SSE coordinates of the nearly equatorial probe orbit in units of lunar radii, and time of day in UT. Periodic spikes in EFI FFT represent probe-shadowing effects, not real plasma waves.

reflecting farther from the tangent point will gain much less energy, since the transformation velocity has a much lower value there. The effect of this energy gain on the electron distribution is shown in schematic form in Figure 2, for an arbitrary loss cone. Note that the energy gain due to reflection from a moving obstacle in general changes a simple loss cone distribution into a conic. The "dispersion" signature therefore likely represents not true velocity dispersion, but rapidly changing reflection efficiency near the tangent point. We discuss the importance of reference frame effects in more detail below in section 2.3.

[11] During magnetically connected intervals, we also observe waves with significant amplitude at a wide range of frequencies. As shown in Figures 1e–1f, we see narrowband waves, with both magnetic and electric field components, at ~100 Hz (as compared to the cyclotron frequency of ~300 Hz). We also find broadband magnetic waves (Figure 1g) extending from 10s of Hz down to near-DC levels, with no obvious peak in frequency. At all frequencies, these broadband waves appear to correlate with intervals of magnetic connection, and with the narrowband waves. Therefore, these waves must either originate near the lunar surface, or result from plasma populations disturbed by the presence of the Moon at the foot point of the magnetic field line.

2.2. Precursor Wave Characteristics

[12] The broadband waves extending from ~0.1–10 Hz in the FGM data match the characteristics of waves observed previously by Lunar Prospector [*Halekas et al.*, 2008a] and Kaguya [*Nakagawa et al.*, 2009]. *Nakagawa et al.* [2009] discussed these waves in detail, and concluded that proton

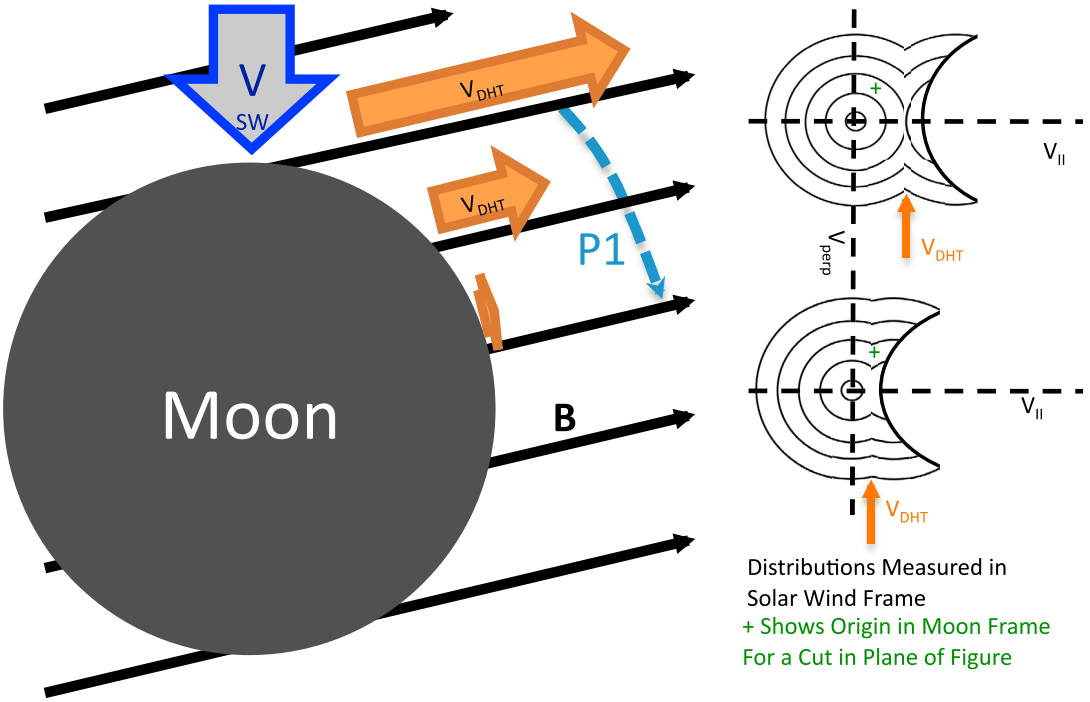

Figure 2. Schematic illustration of magnetic field geometry during the flyby shown in Figure 1, showing the change in the expected deHoffman-Teller frame transformation velocity as magnetic field connection to the lunar surface shifts from the sub-solar point to the flanks, along with sample distribution functions showing the effects of varying deHoffman-Teller velocities on the electron distributions expected on these connected field lines. In the Moon frame, the distribution becomes non-gyrotropic; we show where the origin of the distribution would lie in the Moon frame for a cut through the distribution in the plane of the figure.

reflection from the surface provides the most likely generation mechanism. In this model, the broadband waves would form by cyclotron resonance between reflected protons and right-hand polarized waves blown back over the ions and Doppler shifted to left-handed polarization in the reflected proton frame. Since protons reflect from the surface with a wide variety of angles and energies [*Saito et al.*, 2008], this resonance can generate a broad range of frequencies. While we cannot rule this mechanism out, we note that the broadband waves at this time clearly correlate with intervals of magnetic connection, and with the narrowband waves at higher frequency, suggesting reflected electrons as a more likely culprit. The fact that the broadband waves extend up into the 10s of Hz range in the SCM data also argues for an origin related to electrons. However, both electrons and ions may prove important for generating some or all of these broadband waves, which may prove analogous in some ways to the well-known 1-Hz whistlers seen in foreshock regions at many planets [*Orlowski et al.*, 1990].

[13] In this paper, we focus on the narrowband waves seen near 100 Hz, which we will find have a more obvious origin. We analyze the spectral matrix of fully calibrated SCM waveform data (when available, during wave bursts), rotated into the mean field frame using 20 Hz FGM data, and using a Fourier method to derive the relevant properties of the narrowband waves [*Means*, 1972; *Bortnik et al.*, 2007], and show the results in Figure 3. We find that these waves have a very high degree of polarization (coherency) consistent with their narrowband nature (as an aside, we note that the broadband waves from 10 to 50 Hz have essentially no coherency, though they do show up as a primarily transverse component in the wavenormal-angle spectrum). The narrowband electromagnetic waves also have right-handed, nearly circular, polarization with respect to the magnetic field, and propagate nearly along the magnetic field, consistent with whistler mode.

[14] The polarization analysis leaves us with the usual ambiguity as to parallel or anti-parallel propagation along the field. However, by using EFI and SCM data together, we can resolve this ambiguity. In the inset, we show representative electric and magnetic field waveforms, showing the amplitude-modulated packets characteristic of whistler waves. We find that the Poynting flux points roughly anti-parallel to the magnetic field, indicating that the waves propagate down the field lines toward the Moon. This immediately suggests a cyclotron resonance between outward-traveling electrons and inward-traveling waves [*Neufeld and Wright*, 1964; *Newman et al.*, 1988], and we will see in section 2.4 that this does indeed consistently fit all observations.

2.3. Reflected Electrons

[15] To explain the disturbed electron population upstream from the Moon on connected flux tubes, and the wave activity driven by that population, we must discuss the electron reflection process. The Moon has a distribution of

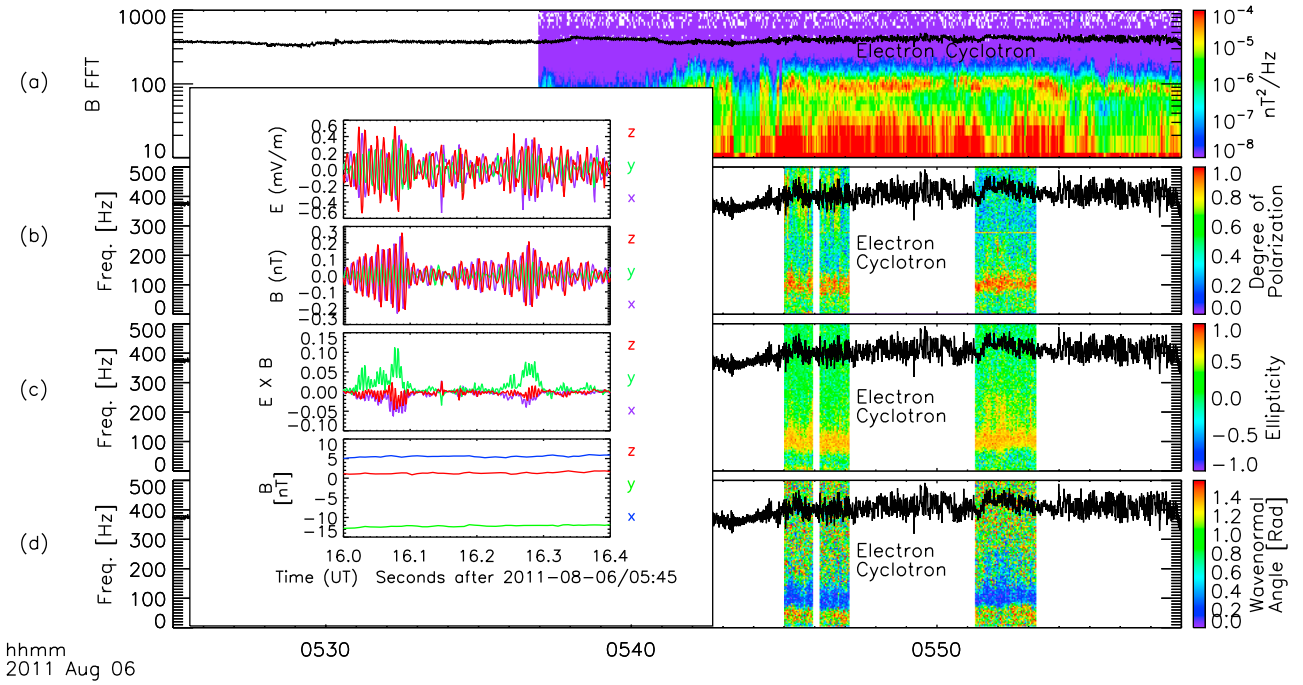

Figure 3. Magnetic field wave polarization analysis for the flyby shown in Figure 1, with (a) spectra of wave power, (b) degree of polarization (1 = perfectly coherent), (c) ellipticity (+1 = right-handed), and (d) un-signed wave-normal angle with respect to the mean field direction (0 = parallel). Inset shows sample electric and magnetic field waveforms (high pass filtered with 50 Hz cutoff), as well as the cross product of the electric and magnetic fields (parallel to the Poynting vector) and the mean field for one interval.

small-scale, but reasonably strong, remanent crustal magnetic fields on its surface [*Mitchell et al.*, 2008], and also has near-surface electrostatic fields resulting from surface charging [*Halekas et al.*, 2008b; *Poppe and Horányi*, 2010], and from solar wind interactions with crustal magnetic fields [*Lue et al.*, 2011; *Saito et al.*, 2012; *Halekas et al.*, 2011b, 2012]. The combined effects of these fields near the surface will reflect some electrons, forming a (generally energy-dependent) loss cone distribution.

[16] Though negative surface charging would enhance reflection efficiency, crustal magnetic fields alone lead to significant reflection, approaching 100% over some regions [*Anderson et al.*, 1975; *Halekas et al.*, 2001]. In addition, the effects of the relative motion between the plasma and the lunar obstacle can boost the reflection efficiency, as discussed above in section 2.1. We now discuss these frame transformation effects in more detail, by considering a representative sample electron distribution in three different reference frames, as shown in Figure 4.

[17] In the Moon frame, the distribution has asymmetry (greatly accentuated by the choice of units) in both the parallel and perpendicular directions with respect to the magnetic field direction, because of the solar wind bulk flow. This holds true in general, since the solar wind velocity can have any angle with respect to the magnetic field. In the Moon frame, the reflection process includes a variety of drifts, and will not conserve kinetic energy, since a convection electric field exists in this frame. In the solar wind frame, on the other hand, the incoming plasma has no bulk velocity and no convection electric field exists. However, since the obstacle moves with respect to this frame at an arbitrary angle, again the reflection process will not conserve kinetic energy, since the electrons gain energy by interacting with the moving obstacle (for some orientations, multiple times). Only in the deHoffman-Teller frame does the reflection process conserve kinetic energy.

[18] We can therefore most easily understand the reflection process in the deHoffman-Teller frame, since it simply consists of adiabatic reflection. Indeed, we see that the measured distribution in this frame has a loss cone in the outward-going direction. Just after reflection, this loss cone should consist of a sharp boundary between electrons that reflect and those that reach the surface. Outside of this loss cone, outward-going fluxes should equal inward-going fluxes at the point in the distribution with the same perpendicular, but opposite parallel velocity. Our measured distribution almost matches this expectation, but has somewhat lower upward-going fluxes than expected outside the loss cone, and appreciable fluxes inside the loss cone. This most likely results from a combination of effects. First, given the small-scale nature of the lunar crustal magnetic fields, reflection may not have a purely adiabatic character even for electrons, reducing the reflection efficiency. Also, the assumption of lateral homogeneity built into the deHoffman-Teller transformation will not hold exactly at the Moon, even on the small electron gyroradius scales. Finally, the loss cone has most likely been "smeared out" by wave-particle effects taking place between the spacecraft and the surface, resulting in lower fluxes outside the original loss cone boundary, and nonzero fluxes inside that boundary.

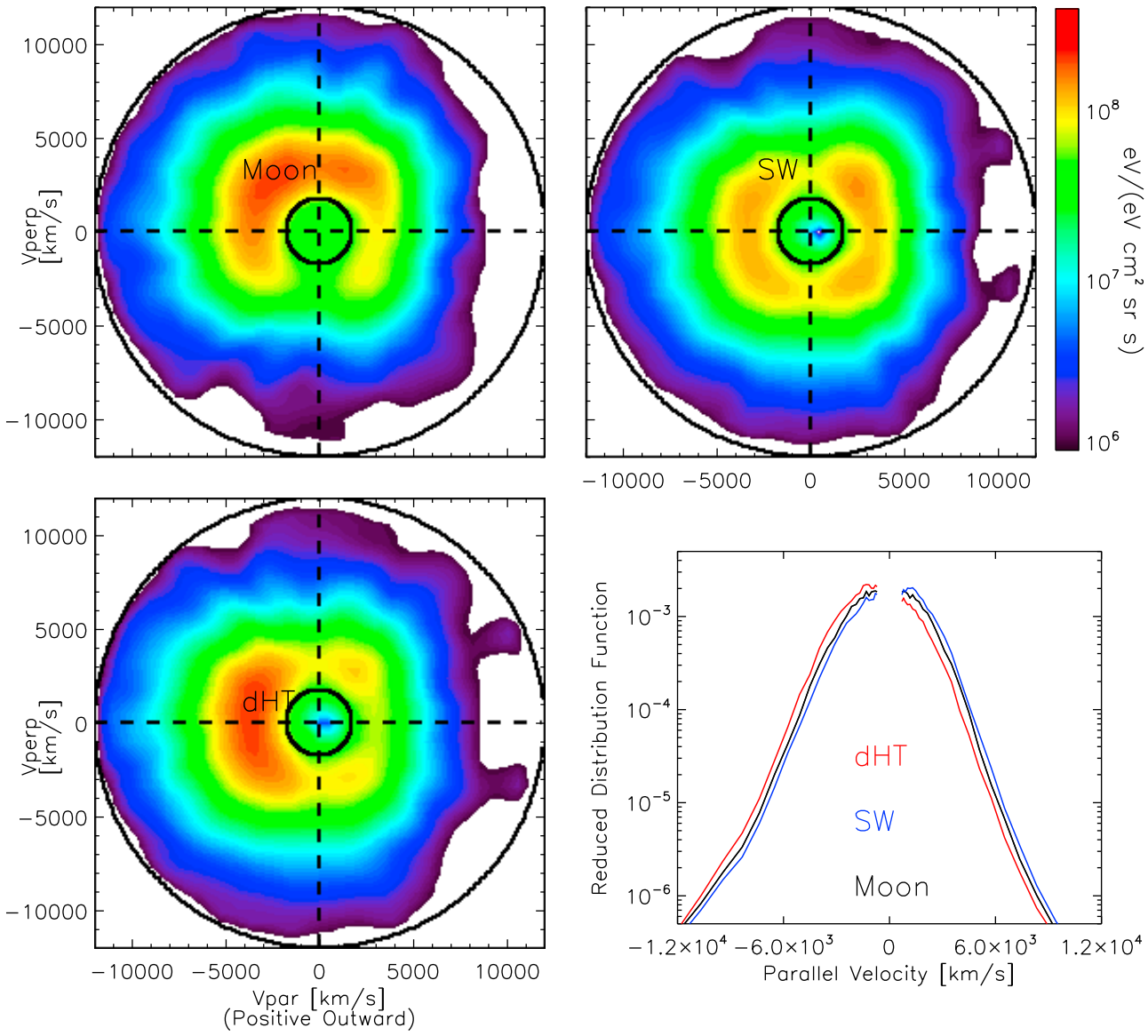

Figure 4. Sample electron distribution function cuts measured at 05:48:00 on August 6th, as a function of parallel and perpendicular velocity, in three different reference frames, and a comparison of the corresponding reduced distribution functions in each reference frame. Inner black circle indicates range of validity of spacecraft potential subtraction and reference frame transformation.

[19] Transforming the distribution to the solar wind frame, we see that the outward-going electrons gain significant energy during the reflection process in this frame (see also the reduced distribution $F(v_{||}) = 2\pi \int f(v_{||}, v_{\perp}) dv_{\perp}$ [where parallel and perpendicular are defined with respect to the magnetic field direction] shown in Figure 4 (bottom right)). This energy boost, resulting from the frame transformation velocity (or, equivalently, from drifts and associated energy gain during the reflection process), transforms the loss cone distribution into a conic, with higher outward-going than inward-going fluxes for some energies, as shown in Figure 2 (top right). The energy gain during reflection from a moving obstacle will produce a highly anisotropic population of outward-going electrons on flux tubes connected to the lunar surface. For the date considered in this paper, we expect to see particularly significant energy gains, since the oblique field orientation ensures a rather large frame transformation velocity, especially near the sub-solar point. Therefore, we can begin to understand the large disturbances, as well as the time-dependence in the reflected electrons when the spacecraft passes flux tubes connected near the sub-solar point (as discussed in section 2.1).

[20] A reviewer noted a slight apparent decrease in flux at small parallel velocities in Figure 4; we have no explanation for this feature, but we note that it is not consistently observed and is not as significant as the features of interest discussed above.

[21] Very similar processes occur near the terrestrial foreshock [*Fitzenreiter et al.*, 1990]. Indeed, the reader may find it surprising that we see such "foreshock-like" processes

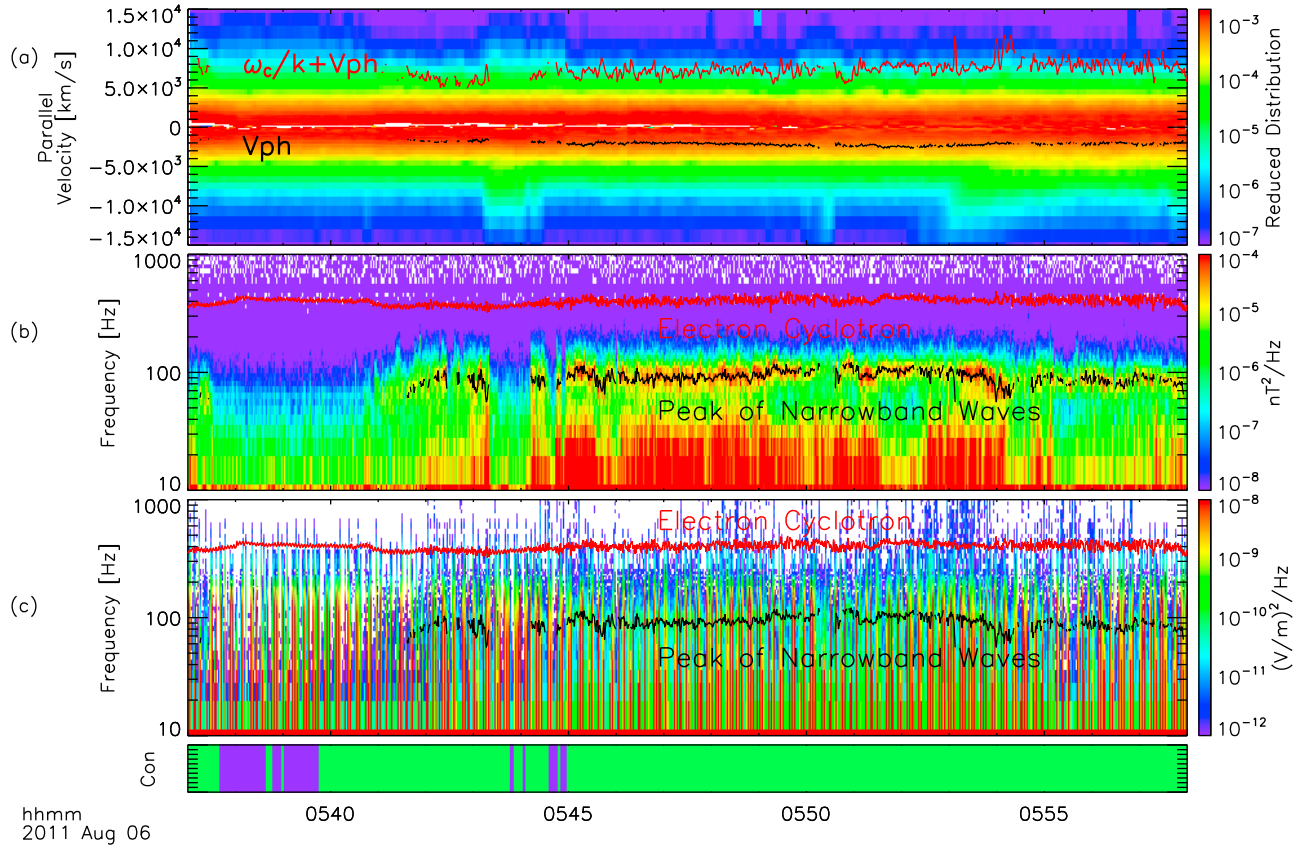

Figure 5. (a) Reduced distribution functions (in solar wind frame) and (b) magnetic and (c) electric field spectra as a function of time for the flyby of Figure 1, with color bar indicating magnetic connection as in Figure 1. Lines in Figure 5a indicate the phase velocity of the narrowband waves assuming they are whistler mode (black), and the parallel velocity of the electrons resonant with those waves (red).

occurring upstream of the Moon, where it remains very much in doubt that true shocks ever form, even over the strongest crustal magnetic field sources. However, in fact we need only have a generalized obstacle with electromagnetic fields capable of reflecting some particles to observe such phenomena. Indeed, the Moon may present a very unique opportunity to study some phenomena normally observed only in the foreshock, but with an actual shock completely absent. This unique aspect of the lunar environment could help us to differentiate between processes that occur in the shock and propagate outward, and those that simply result from reflected particle populations.

2.4. Precursor Whistler Wave Generation

[22] We now consider the generation mechanism for the narrowband ~100 Hz whistlers, which we suspect to result from the reflected electron population described above. The anisotropy of the reflected electrons (in particular, the positive $df/dv_\perp$ of the loss cone) will drive wave growth [*Kennell and Petschek*, 1966; *Wu et al.*, 1983]. As a useful way of showing the resonance condition, we show wave spectra together with the reduced electron distribution functions, as a function of time, in Figure 5. We hypothesize that the waves result from a cyclotron resonance between outward-going electrons and inward-going waves. For this to occur we must have $v_\parallel = \omega_{ce}/k + v_{ph}$ for the resonant electrons. The waves also must satisfy the local whistler dispersion relationship, which we approximate by the cold plasma dispersion relationship for parallel-propagating right-hand polarized waves $k^2c^2 = (\omega^2 - \omega\omega_{ce} - \omega_{pe}^2)/(1 - \omega_{ce}/\omega)$. We solve the latter equation for the wave number k using measured quantities for the peak wave frequency and the other variables, and also show the derived phase velocity and the resulting resonant parallel velocity in Figure 5a. The derived wave numbers imply parallel wavelengths on the order of ~20 km. Strictly speaking, we should take into account the Doppler shift between the spacecraft frame and the solar wind frame, and solve the Doppler shift equation together with the whistler dispersion relation, but in this case we can safely neglect this subtlety since the wave phase velocity of a few thousand km/s greatly exceeds the solar wind velocity component along the magnetic field (a few hundred km/s or less).

[23] Figure 5a shows that the peak of the narrowband waves meets the cyclotron resonance conditions for parallel electron velocities corresponding to the upper edge of the range of significant outward-going electron fluxes. We can now begin to understand why the whistlers have a relatively narrowband character. Waves at lower frequencies would resonate with larger parallel outward-going electron velocities; in fact, few electrons exist at larger outward-going velocities, so the wave power drops off below the lower edge of the wave band. Meanwhile, waves at higher frequencies correspond to smaller parallel outward-going

electron velocities. At smaller parallel velocities, only electrons with fairly small perpendicular velocities (near the loss cone edge) have anisotropy with the right sense to drive wave growth. Instead, most of the electrons at these smaller parallel velocities have perpendicular velocities outside of the loss cone, without the required anisotropy, and contribute to cyclotron damping of the wave rather than driving wave growth. This roughly corresponds to the rule of thumb that cyclotron damping inhibits significant wave growth when the resonant velocity lies below the phase velocity in magnitude (or equivalently, for the scenario in question, when the resonant frequency exceeds half the electron cyclotron frequency) [*Stix*, 1962]. In the solar wind, we do not observe obvious perpendicular heating resulting from this cyclotron damping, but in the magnetosphere we will find that we can easily observe the results of the damping process.

[24] We now recognize that the narrowband whistlers in the upstream precursor region grow from the anisotropy of the loss cone in the reflected electron distribution, and act to remove anisotropy from that distribution. This process has likely already smeared out the electron distribution to some degree at the spacecraft location, by filling in the loss cone and smoothing out any sharp boundary in the distribution, as we saw in Figure 4. Wave growth should continue on connected flux tubes at larger distances from the Moon, since significant anisotropy remains in the distribution; however, we can expect the wave amplitude to decay with altitude.

[25] The narrowband waves cease at several times. Wave growth stops every time the rotation of the magnetic field breaks connection to the surface, as for example just before 5:45. This obviously occurs because the source of the wave growth disappears when the connection breaks. In addition, the wave growth ceases at some of the times when the dispersed inward-going electron bursts indicate magnetic connection to the terrestrial foreshock. We hypothesize that the incoming electron bursts modify the dispersion relation from the cold plasma dispersion relation enough to break the resonance condition and shut off wave growth. However, one might also speculate about the potential for interesting feedback processes on flux tubes connected at one end to the Moon and at the other to the terrestrial foreshock.

3. Lunar Precursor Observations in the Terrestrial Magnetosphere

3.1. Overview of Magnetosphere Observations

[26] We now proceed to discuss similar observations in the terrestrial magnetotail, where we will find many analogous phenomena, but also several additional features of note unique to this very different environment. Figure 6 shows an overview of a lunar flyby in the magnetotail, in the same format as Figure 1. The ambient plasma environment differs greatly from that in the solar wind. The plasma temperature for both electrons and ions exceeds the bulk flow energy, and the magnetic field has fairly steady, but not quite lobe-like characteristics, indicating a probable location in the plasma sheet near the lobe. Nonetheless, we see many of the same features that we saw the solar wind (but, in general, more accentuated).

[27] As in the solar wind, we see few obvious effects of the Moon's presence in the omni-directional ion spectra in Figure 6a (we will see some shadowing effects in pitch angle spectra in section 3.6). However, in the omni-directional electron spectra in Figure 6b, we clearly see two populations. By looking at the parallel and anti-parallel spectra in Figures 6c and 6d, we find that these consist of a hot Moonward-going population, and a cold outward-going electron beam with very high fluxes. This beam varies in energy, but persists over nearly the entire time period.

[28] Particularly at times when this beam has higher energy (11:53–11:58, 12:02–12:12), we observe a variety of wave modes. We see broadband electrostatic wave power extending up to the plasma frequency (Figure 6e). And, we see narrowband electromagnetic waves near 100 Hz (Figure 6f), just as we did in the solar wind.

[29] Finally, in the low frequency magnetic field in Figure 6g, though we find none of the broadband turbulence we saw in the solar wind, we do observe a burst of wave power near the local proton cyclotron frequency. These low frequency waves, seen when the spacecraft passes through flux tubes connected near the sub-solar point (as indicated in the legend at the bottom of Figure 6), clearly modulate the narrowband electromagnetic waves.

3.2. Precursor Wave Characteristics

[30] We naturally suspect that similar mechanisms to those seen in the solar wind must generate the narrowband electromagnetic waves. And, indeed, we see in Figure 7 that these waves have exactly the same characteristics as the narrowband whistlers in the solar wind. They have high coherency, right-hand polarization with respect to the magnetic field, and they propagate in the anti-parallel direction along the magnetic field (toward the Moon). We find a somewhat higher E/B ratio in the magnetosphere than in the solar wind, indicating a higher phase velocity, and also a larger Poynting flux. Other than these small differences, though, the characteristics of these waves appear very similar to those seen in the solar wind, suggesting a similar origin.

3.3. Reflected and Accelerated Electrons

[31] Unlike in the solar wind, the electrons in the magnetosphere have fairly clear and distinct boundaries in phase space (though still not perfectly sharp, indicating that some wave-particle interactions have occurred). We show three sample distributions in Figure 8, spanning the range of observations during this time period. The first two distributions, measured during periods of significant narrowband electromagnetic wave growth, have very similar features. In particular, they have a clear loss cone distribution, with an outward-going electron beam superposed on this distribution. The loss cone distribution must result from reflection from crustal magnetic fields near the surface. The beam consists of secondary and/or photoelectrons produced at the surface, and accelerated through a non-monotonic surface potential layer, as observed previously by both Lunar Prospector [*Halekas et al.*, 2005, 2008b; *Poppe et al.*, 2011] and ARTEMIS [*Halekas et al.*, 2011a]. *Poppe et al.* [2012] have presented detailed model-data comparisons for this date, so we will not discuss the electron beam in detail, other than to mention that it may ultimately exist in order to help maintain

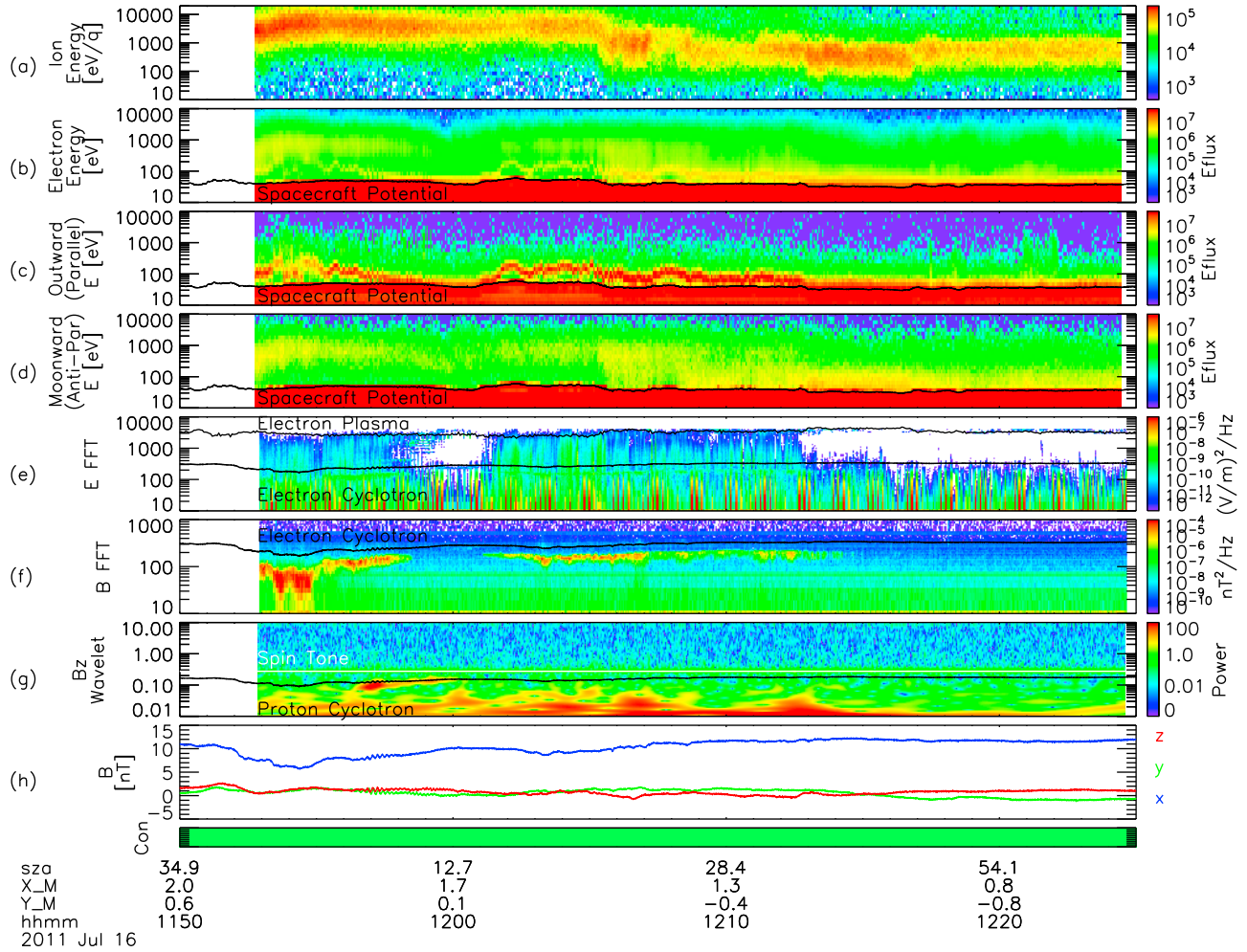

Figure 6. Data from an ARTEMIS P1 lunar flyby in the terrestrial magnetosphere on July 16th, 2011. All panels same as Figure 1. Black lines on energy spectra indicate the spacecraft potential, separating plasma electrons from spacecraft photoelectrons. Top black line on EFI FFT indicates the plasma frequency. White line on magnetic field wavelet indicates the spin frequency.

quasi-neutrality on flux tubes upstream from the Moon [*Halekas et al.*, 2011a, 2012]. We note that the beam has high enough flux and a sharp enough peak to produce a positive slope even in the reduced distribution (Figure 8, bottom right), indicating that electrostatic beam modes have not yet produced a plateau in the distribution. The high level of broadband electrostatic wave power at these times most likely results from streaming instabilities driven by these beams.

[32] The third distribution was measured at a time with no significant wave growth, and has no significant reflected flux (in other words, a 90° loss cone angle, or a loss cone that extends to cover the entire outward-going half of the distribution). At this time, the spacecraft passes flux tubes connected to a region of the surface without significant crustal magnetic fields, so no loss cone exists. A vestige of an upward-going beam does still exist at velocities of a few thousand km/s, though it has rather low energy (below 10 eV), as expected given the lower ambient electron temperature. At this time, we see no clear peak in the reduced distribution, also consistent with the lack of electrostatic wave power at this time. We note that the lack of electromagnetic waves at this time (despite the presence of the weak beam) may help confirm that the loss cone rather than the beam provides the key driver of the whistlers, as expected since it has anisotropy in the correct sense. However, given the weakness of the beam, we cannot conclusively state this.

[33] As a final aside, we note that the first distribution, measured at 11:57, shows signs of significant perpendicular heating at low parallel velocities. We will see in section 3.6 that we observe this feature at all times with significant narrowband electromagnetic wave power. This heating likely results from cyclotron damping. At low parallel velocities, though a portion of the distribution may drive wave growth, a larger population absorbs electromagnetic waves. The anisotropy in the loss cone at low parallel and perpendicular velocities can generate waves, just as it does at higher outward-going parallel velocities, but the bulk of the population at low parallel velocities lies outside of the loss cone, and this population re-absorbs these waves [*Thorne and Horne*, 1996], gaining perpendicular energy in the

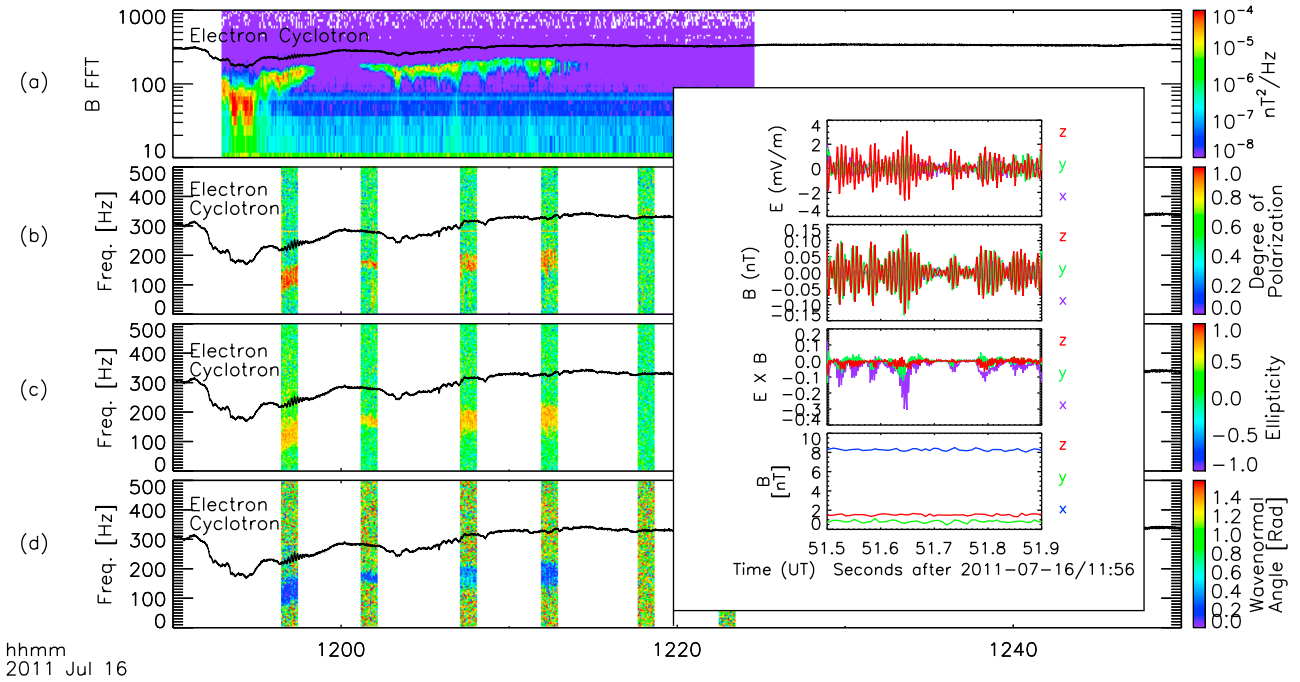

Figure 7. Magnetic field wave polarization analysis for the flyby shown in Figure 6. All panels same as Figure 2.

process. As discussed in section 2.4, this damping helps explain the narrowband nature of the waves. The resulting anisotropy at low parallel velocities might itself drive additional waves, possibly producing some of the electrostatic power we observe, and leading to interesting feedback processes.

3.4. Precursor Whistler and Electrostatic Wave Generation

[34] Though we can already feel fairly confident that the loss cone anisotropy generates the precursor whistler waves in the magnetosphere, as it does in the solar wind, we repeat the same analysis as in Section. 2.4, and show the results in Figure 9. Again, we find that the electrons at the very upper edge of the upward-going loss cone and the peak of the narrowband waves meet the resonance condition. In the magnetosphere, with much larger spatial/temporal variations in electron temperature and other parameters, the correspondence between the electrons and the waves over a wide range of different ambient conditions proves even more striking.

[35] In this case, despite the similar wave frequencies, the parallel phase velocity has a much higher magnitude, as already indicated by the E/B ratios seen in Figure 7. This results primarily from the much lower plasma frequency in the low-density magnetotail environment, which changes the whistler dispersion relationship. This also implies a larger parallel wavelength, on the order of ~100 km, as compared to ~20 km for the solar wind case.

[36] Though the narrowband electromagnetic wave characteristics prove very similar to those in the solar wind, the electrostatic waves differ significantly. While we saw few electrostatic modes in the solar wind, we see significant broadband electrostatic power extending up to the plasma frequency in the magnetosphere. At most of the times where we see these waves, the outward-going reduced electron distribution clearly has a positive slope, as seen in Figure 9a, strongly suggesting a beam mode. Electron acoustic modes [*Gary*, 1987] could also grow, but we would expect these to have lower growth rates. In addition, we see some evidence for electrostatic electron cyclotron waves, and even electron cyclotron harmonics, from 11:58–12:01.

[37] Nearly all wave growth ceases after 12:12, though magnetic connection to the surface persists throughout the interval. As suggested above, this shutoff must result from changes in the upward-going electron distribution. No significant magnetic reflection occurs over most of this interval, and the upward-going beam has low energy and has already developed a plateau. Intriguingly, at 12:18 and again at 12:22 the spacecraft passes flux tubes connected to significant crustal magnetic field sources (one of them is the well known Reiner-Gamma anomaly, one of the strongest on the Moon). However, though we see a brief renewal of significant upward-going fluxes at these times, we observe no corresponding renewal of wave growth. Possibly, the strong crustal magnetic fields produce a loss cone so narrow that it cannot drive significant waves. Alternatively, the narrow loss cone may already have filled by the time the electrons reach the observation point, and no longer has anisotropy sufficient to drive waves.

3.5. Precursor Wave Modulation by ULF Effects

[38] As noted in Section 3.1, we observe a short burst of ULF waves near the proton cyclotron frequency when the spacecraft passes flux tubes connected to the surface near the sub-solar point at ~11:56–12:00 (Figure 6g). We show more details of this time period in Figure 10. We observe the ULF waves first with both compressional and transverse

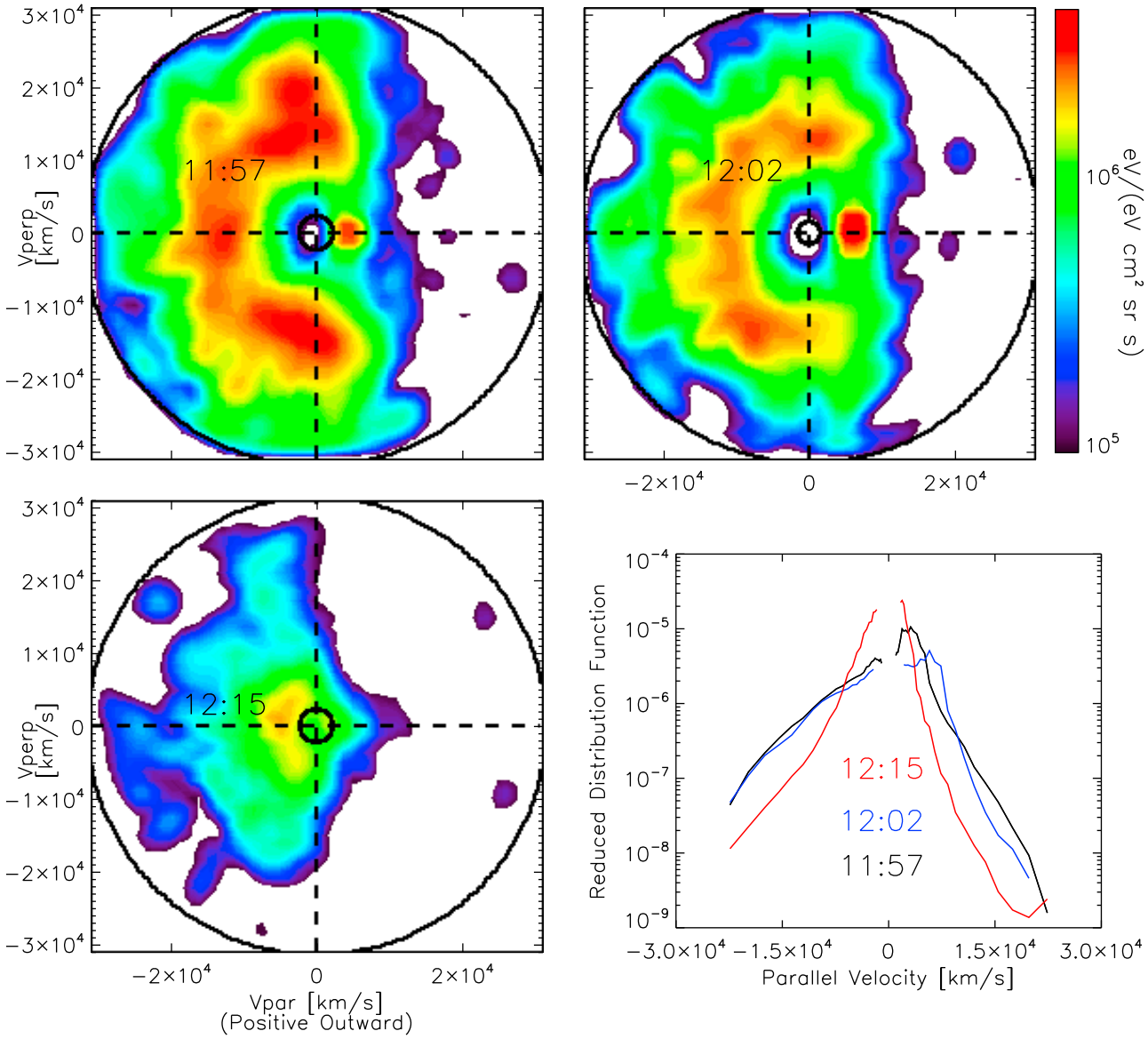

Figure 8. Sample electron distribution function cuts for three different times, all in Moon frame, during the flyby of Figure 6, in same format as Figure 3.

components from 11:56–11:58, and then later with a primarily transverse nature from 11:58–12:00. They track the proton cyclotron frequency very well, as it varies over a factor of two. We also find some indications of a secondary peak in the transverse wave power near the He+ cyclotron frequency, though with less wave power than the primary peak. The ULF waves persist after the whistlers cease, and only occur for a few minutes out of the interval during which we do observe the whistlers, so they do not likely arise from the same population of particles.

[39] The partly compressional nature of the ULF waves also manifests in the plasma density. The spacecraft potential provides the highest time resolution measure we have of the plasma density. Given relatively constant plasma temperature, the spacecraft potential has an inverse dependence on plasma density, as a result of the balance between plasma and photoelectron currents. When plasma density increases, the spacecraft potential goes down, since more photoelectron current must escape the spacecraft sheath in order to balance the incoming electron current. When the plasma density decreases, conversely, the spacecraft potential must go up in order to trap more photoelectrons and quench the escaping photoelectron current. In this case, we find that the spacecraft potential varies in phase with the magnetic field magnitude, implying that the plasma density varies in an opposite sense to the magnetic field magnitude. Thus, the compressional part of this wave could have mirror mode (given circular polarization, this appears highly doubtful) or slow mode characteristics, but not fast mode.

[40] The ULF waves clearly modulate both the amplitude and frequency of the whistlers. The frequency modulation could result from the modulation of the electron cyclotron frequency, and the resulting change in the resonance conditions. However, the whistler modulation appears slightly out

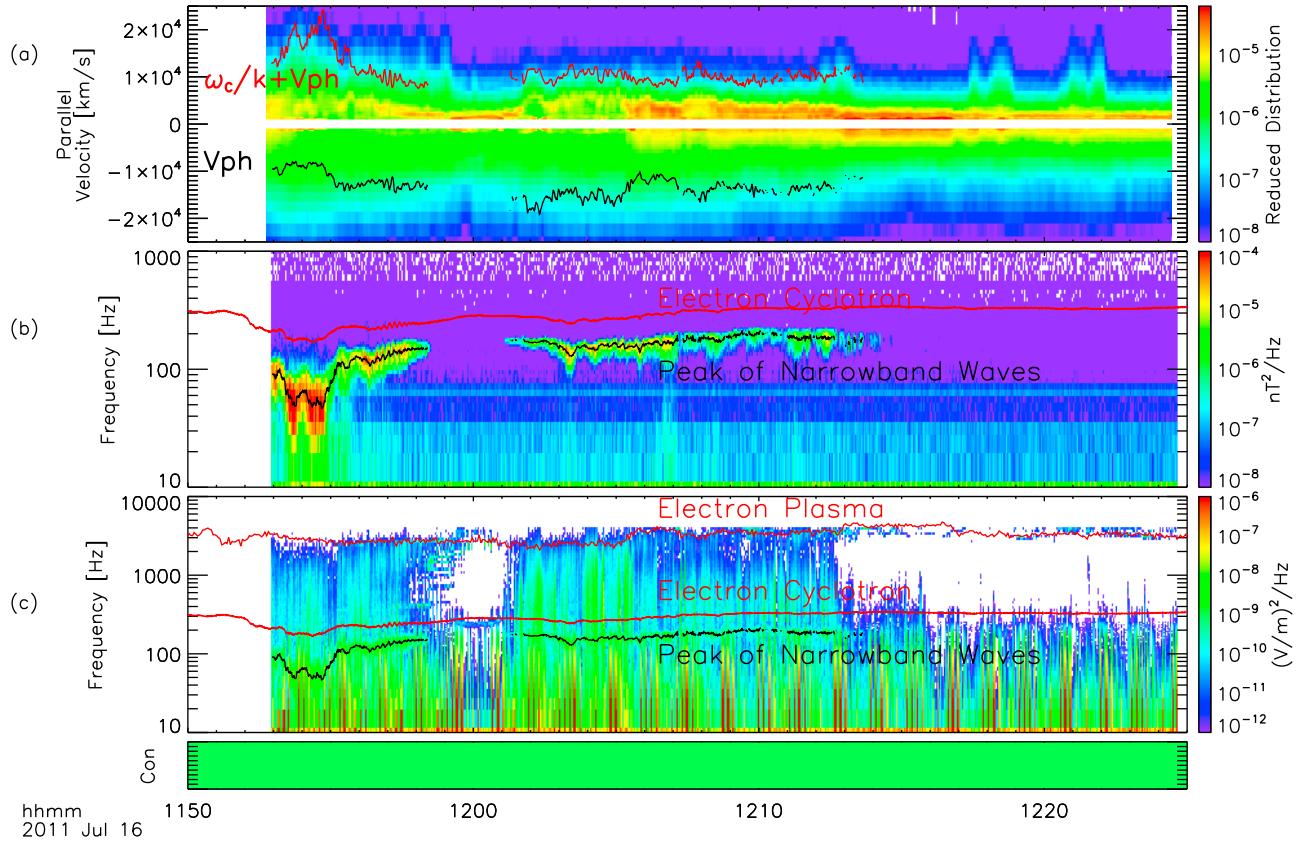

Figure 9. Reduced distribution function (in Moon frame) and magnetic and electric field spectra as a function of time for the flyby of Figure 6. All panels same as Figure 5.

of phase from the ULF waves at the spacecraft location (as seen using the vertical line as a tracer), which could indicate a delay related to propagation effects and might point to a non-local generation mechanism for one of the wave modes. The amplitude variation of the whistlers seems somewhat harder to explain. Possibly, this simply relates to density changes associated with the compressional nature of the wave, as seen for the very similar magnetospheric chorus waves [*Li et al.*, 2011]. However, the amplitude modulation also appears out of phase with both the density modulation and the frequency modulation, possibly indicating some nonlinearity. The rising tones and the slow rise and then sharp decrease in wave amplitude seen from 11:56–11:58 could also indicate a nonlinear wave growth mechanism and saturation effects. As an alternate explanation, the ULF waves could simply change the location of magnetic field connection to a point with different electrostatic potentials, thus modulating both electrons and waves.

3.6. Precursor Wave Effects on Charged Particles

[41] We now look in more detail at the characteristics of the charged particles observed during the most interesting part of this event, showing pitch angle distributions for several different energy ranges for both the electrons and the ions in Figure 11. In the lowest electron energies (Figure 11i), we see the outward-going electron beam (at pitch angles near zero) when clearly separated from the spacecraft photoelectrons before 11:59 and after 12:01) that drives the electrostatic modes, while in the higher energies (Figures 11g–11h) we see the loss cone that drives the whistlers. We note that the ULF waves clearly modulate not only the whistlers, but also the electrons. Both the outward-going electron beam energy and the loss cone width show significant modulation. All of these characteristics suggest that a nonlinear wave growth mechanism and/or coupling between multiple populations and waves must play a significant role. It appears likely that the ULF waves couple strongly to the electrons and may modulate their energies and fluxes, probably via parallel electric fields associated with the wave, as observed in terrestrial auroral regions [*Temerin et al.*, 1986; *McFadden et al.*, 1998]. This modulation of the electrons may help explain the out of phase modulation of the whistlers discussed in the previous section.

[42] We also note that the perpendicular electron heating at low parallel velocities seen in Figure 8 and discussed in section 3.3 shows up in the spectra as a band around 90° pitch angle from 11:56–11:59 and from 12:01–12:04 in the highest energy range (Figure 11g). This band persists for the entire time period when we observe the narrowband whistlers. As discussed above, this population likely results from cyclotron damping of whistlers generated with frequencies higher than the band where we observe the peak wave power. Those higher frequencies correspond to waves resonant with electrons with smaller parallel velocities, few of which have anisotropy in the correct sense to generate waves, with the bulk of these electrons having perpendicular

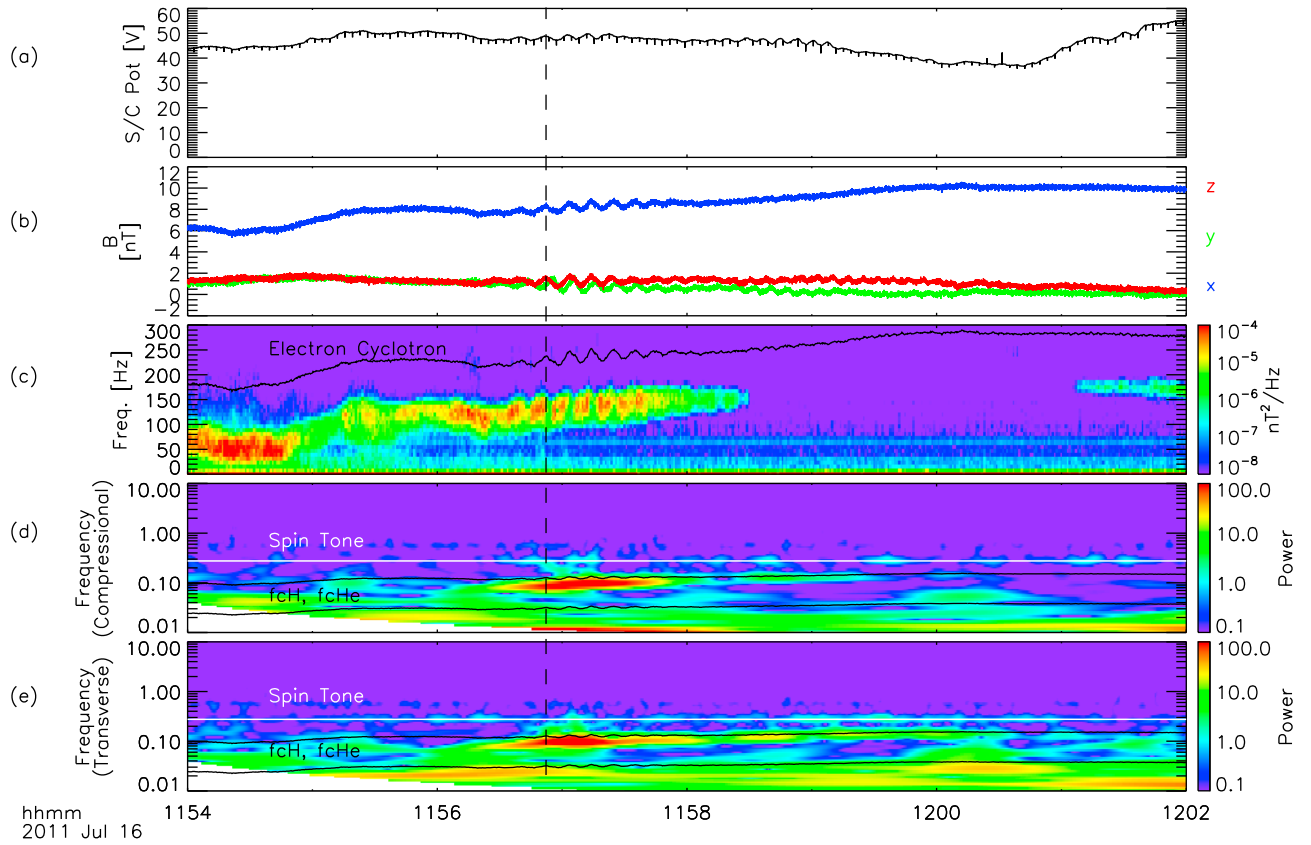

Figure 10. Overview of ion scale waves seen during the flyby of Figure 6, showing (a) spacecraft potential (as a proxy for plasma density), (b) magnetic field components in SSE, (c) high frequency magnetic field power spectra from the SCM, and (d) compressional and (e) transverse low frequency power spectra from the FGM. White line in Figures 10d and 10e indicates the spin frequency, while the two black lines show the proton and helium cyclotron frequencies.

velocities lying outside the loss cone and rapidly damping any waves that grow, as discussed previously.

[43] The ion pitch angle distributions also display several interesting features. At medium energies (Figure 11b), the ions have a clear loss cone, showing the results of a combination of somewhat non-adiabatic (given the significant ratio of ion gyroradius to crustal field scale size) magnetic reflection and simple shadowing by the solid obstacle. At these energies, the ion loss cone lies close to the electron loss cone, implying mostly relatively adiabatic reflection.

[44] At higher energies (Figure 11a), we also observe a loss cone, but with an additional lower flux population inside the loss cone near pitch angles of 60 degrees. This population corresponds to ions that have large enough energies (and thus, large enough gyroradii) for some ions to gyrate around the Moon and reach the observation location near the sub-solar point. The resulting ion anisotropy could generate waves [*Davidson and Ogden*, 1975], but it does not correlate well with any of the observable ULF waves other than perhaps those near the He+ cylotron frequency. Also, ion anisotropy exists to some degree over the entire time range, so some other element must also factor into the conditions for wave growth at this time in order to explain the observations.

[45] Finally, in the lowest energy ion band (Figure 11c), we see very few ions, except around 12:00, when we observe a faint population of ions at 90° pitch angle. These could represent newly picked up gyrating ions of lunar origin, perhaps even those responsible for driving the ULF waves. However, they appear offset in location from the strongest waves at the proton gyrofrequency, casting doubt on this interpretation. On the other hand, they do appear near a peak in ULF wave power near the He+ gyrofrequency, suggesting a possible identification as He+ ions that locally produce ion cyclotron waves.

3.7. Precursor ULF Wave Generation

[46] Numerous mechanisms, a few already mentioned, could generate the ULF waves. Ions of lunar origin provide one interesting possibility. During the time period of peak ULF wave power (11:56–11:58), the plasma has no significant bulk flow and the spacecraft passes flux tubes connected to the surface near the sub-solar point. In this location, ionized exospheric constituents [*Stern*, 1999] or sputtering products [*Yokota et al.*, 2009; *Tanaka et al.*, 2009] could build up near the Moon's surface, escaping primarily along the magnetic field lines at slow speeds, rather than following the pickup ion trajectories expected at times with more significant perpendicular electric fields. Absent electric field acceleration, we could not easily observe these ions directly, since their initial energy lies well below the ESA energy range, especially taking into account the large positive

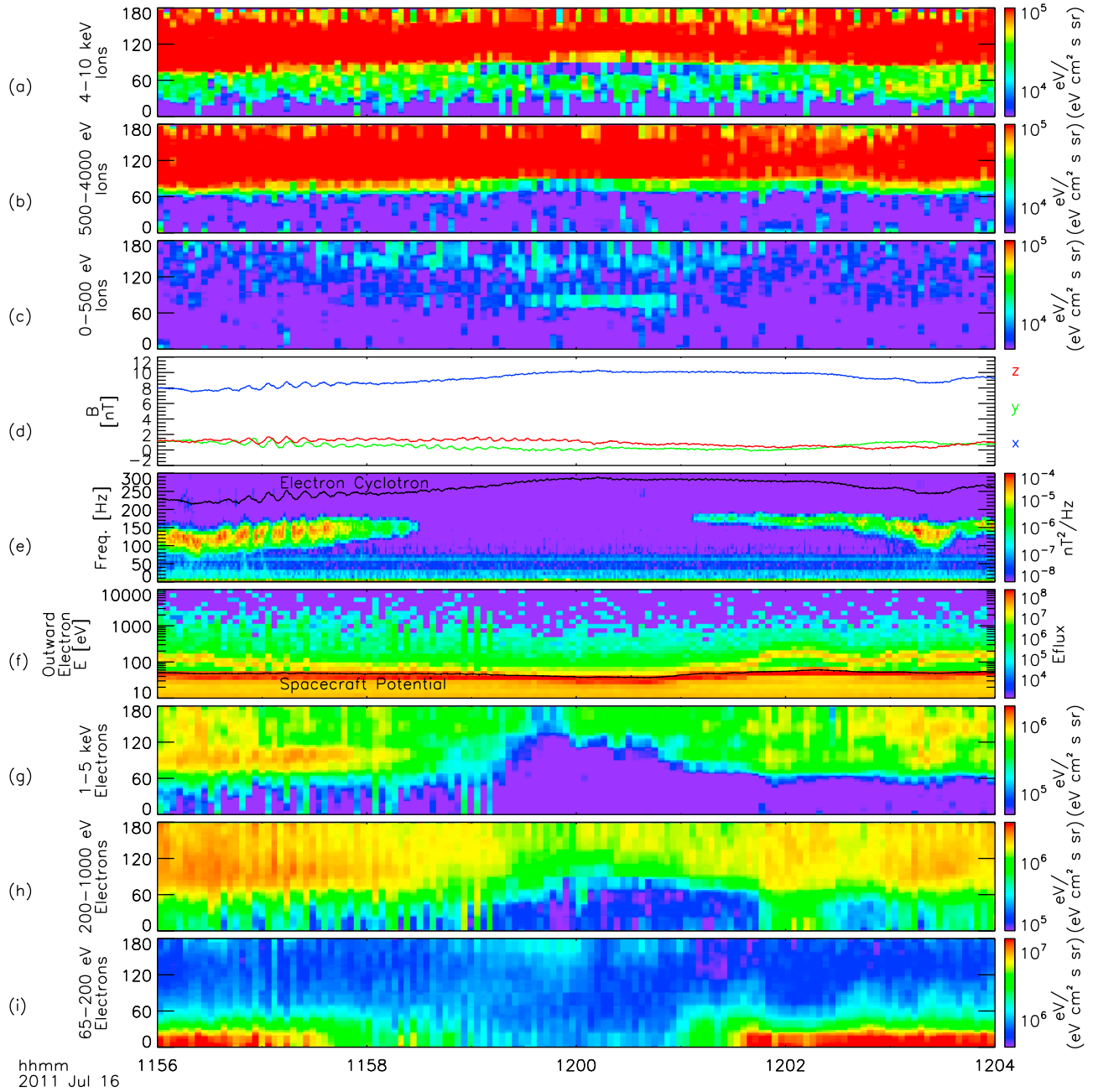

Figure 11. Particle distributions for the flyby of Figure 6, showing (a–c) ion pitch angle spectra for three energy ranges, (d) magnetic field components in SSE, (e) magnetic field power spectrum, (f) electron energy spectra, and (g–i) electron pitch angle spectra for three energy ranges. All particle spectra have units of differential energy flux (eV/[eV cm^2 sr s]).

spacecraft potential. These ions would build up a density/pressure enhancement above the lunar sub-solar point. The resulting parallel pressure gradient could drive a slow mode wave, but this would not easily explain the relatively high frequency, the large number of wave periods observed, or the peak at the ion cyclotron frequency of the waves we do see.

[47] One attractive possibility associated with the presence of lunar ions relates to the bi-ion modes produced by the interaction of multiple ion populations. Ion populations streaming relative to each other can produce electromagnetic ion cyclotron (EMIC) waves [*Winske and Omidi*, 1992], and this holds for populations of different species as well. The AMPTE Barium release provides a particularly interesting comparison; in this case, researchers attempted to explain the observed waves in terms of bi-ion streaming between the solar wind and newly born Ba+ ions that generated waves at higher frequency, which were then Doppler shifted and observed near the proton cyclotron frequency and one fifth of that frequency [*Sauer et al.*, 1999], rather similar to our observations. The ion population in the magnetosphere has significantly different characteristics from that in the solar wind, making it difficult to extrapolate from one scenario to

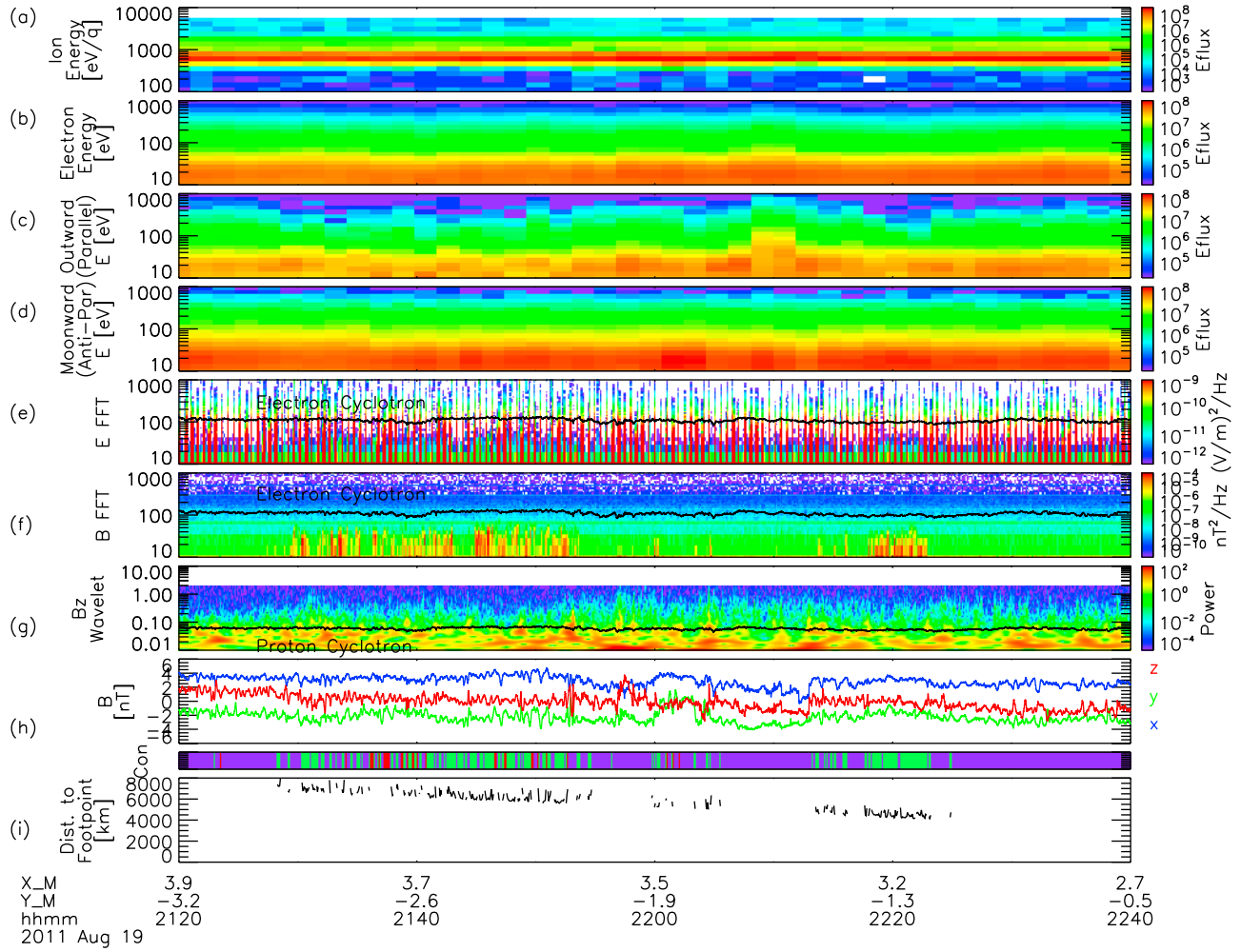

Figure 12. Data from an ARTEMIS P2 lunar flyby in the solar wind on August 19th, 2011. All panels same as Figures 1 and 6, except for the addition of Figure 12i showing the distance along the field line to the foot point at times of magnetic field connection to the lunar surface.

the other. Finally, we note that the presence of the electron beam itself, coupled with bi-ion modes, could help drive wave growth, as postulated in the terrestrial auroral region [*Temerin and Lysak*, 1984]. This would help explain the modulation of the electron beam by the ULF waves, as discussed above. The biggest outstanding question with all of these possibilities, of course, remains the very close association with the local proton cyclotron frequency.

[48] We cannot rule out the possibility that a convection electric field sufficient to pick up the ions actually does exist, or that the cross-tail electric field could play this role. In this case, the situation might have close analogies to cometary environments, where pickup ions form a ring beam distribution and drive waves near cometary ion gyrofrequencies [*Glassmeier and Neubauer*, 1993; *Tsurutani et al.*, 1989]. These waves can even have a compressive nature [*Mazelle et al.*, 1997]. However, we would not expect to see a peak at the H^+ or the He+ gyrofrequency near the Moon. Though the lunar exosphere has significant neutral H and He, their long photo-ionization lifetimes would make observations of significant H^+ or He+ densities near the Moon surprising. Furthermore, we would expect to directly observe a significant gyrating pickup ion population in this case, so we do not favor this explanation.

[49] In the final analysis, we suspect that lunar ions may play a role in generating the observed ULF waves, but we cannot conclusively settle on a mechanism. We also cannot rule out wave growth related to the anisotropy produced by the complicated pitch angle and energy dependent shadowing of the ions; however, the duration of this effect greatly exceeds the length of the time period where we see low frequency waves. Meanwhile, the modulation of the electrons suggests that the electron beam might also play a role, but it could merely indicate the secondary effects of parallel electric fields associated with the low frequency waves. Regardless, the fact that we only observe the ULF waves for a short time suggests that some other factor, such as the buildup of lunar ions near the sub-solar point discussed above, must play an important role.

4. Implications

[50] The observations we have presented in this paper, together with the large existing body of observations from

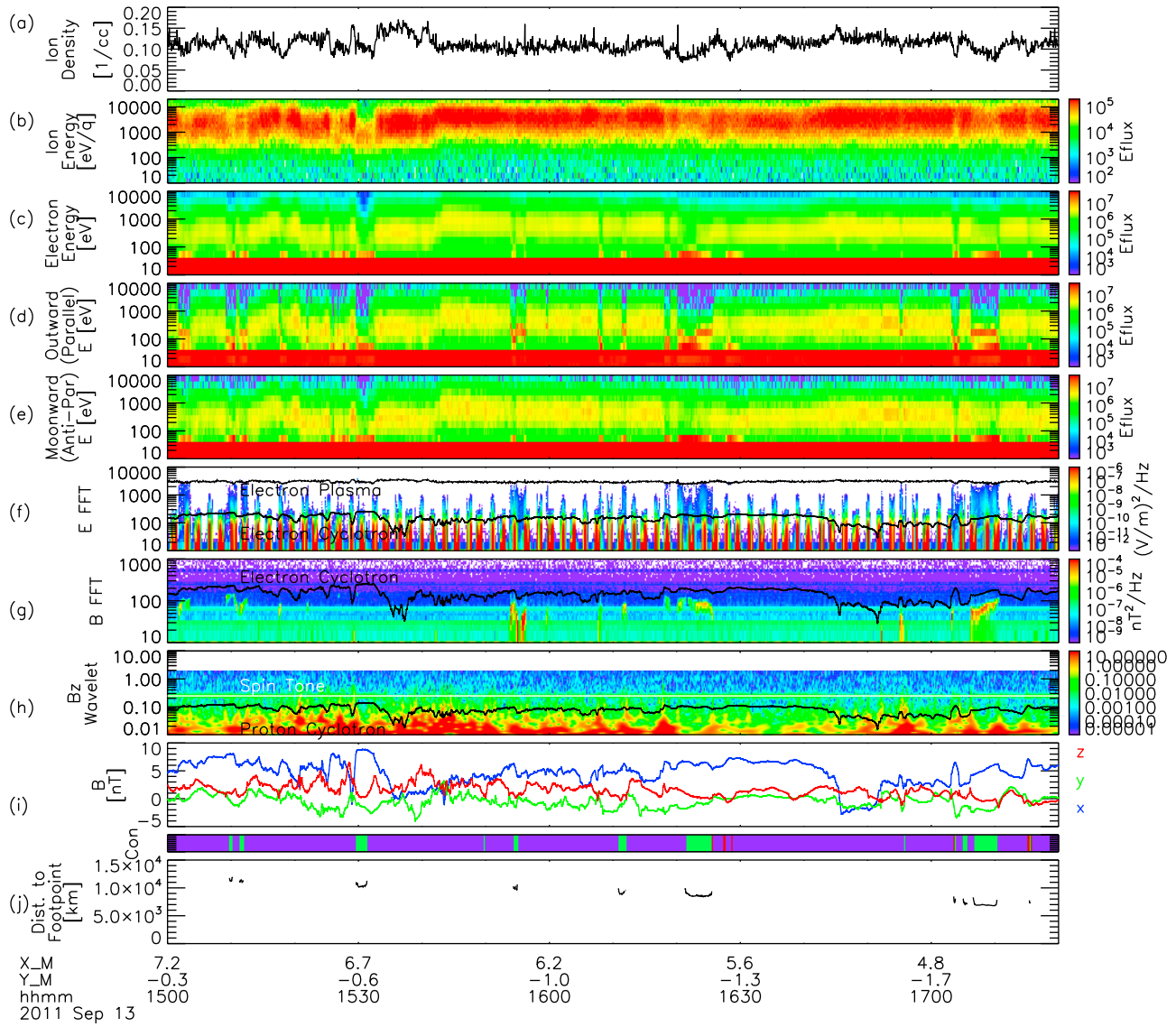

Figure 13. Data from an ARTEMIS P1 lunar flyby in the terrestrial magnetosphere on September 13th, 2011. All panels same as Figure 12, except for the addition of the Figure 13a showing the ion density.

Wind, Kaguya, Chandrayaan, Chang'E, and other spacecraft, paint a picture of a disturbed region upstream from the Moon, existing mainly on magnetic field lines connected to the dayside surface (also to the wake). We have shown that a number of the effects seen in this region have clear analogies to terrestrial foreshock processes. In some sense, it appears that the Moon has an "electron foreshock" of its own, though (at least for most plasma conditions) it has no actual shock. The Moon therefore provides a unique environment in which to investigate fundamental plasma processes, especially wave-particle interactions.

[51] We close by considering the question "At what distance can the ambient plasma feel the presence of the Moon"? We present two sets of observations, one from P2 in the solar wind in Figure 12, and one from P1 in the terrestrial magnetosphere in Figure 13, spanning the range of distances over which we have so far observed lunar precursor effects with ARTEMIS.

[52] The solar wind observations in Figure 12, taken at a GSE location of [−23, −60, 4] earth radii, just outside of the terrestrial bow shock, have many of the same characteristics as the case discussed in Section 2, but at much greater distances from the lunar surface. We see some ULF waves below the proton cyclotron frequency (Figure 12g), but uncorrelated with magnetic connection, indicating that they probably result from terrestrial foreshock processes. However, the P2 probe, passing the Moon on the side opposite the Earth and thus partially shielded from terrestrial foreshock effects, also observes electromagnetic waves up to ∼50 Hz whenever it passes through flux tubes connected to the surface. Consistent with the lower electron cyclotron frequency during this time, these extend to lower frequencies than those previously discussed and have less of a narrowband character, but they almost certainly result from the same loss cone anisotropy mechanism. We observe these waves, along with disturbed electron distributions, at

distances of up to ~8,000 km from the surface, with little apparent reduction in wave power. The parallel (outward-going) electrons (Figure 12c) show signs of disturbances throughout the interval, because when the Moon does not intersect the field line and the spacecraft is thus not magnetically connected to the lunar surface, the spacecraft is instead magnetically connected to the terrestrial foreshock. Indeed, the characteristics of the outward-going electrons on field lines connected to the foreshock appear fairly similar to those on field lines connected to the lunar surface, yet again pointing to the similarity between the two regimes. However, the foreshock electrons do not have a loss cone, so only during the intervals of connection to the Moon do we observe the electromagnetic precursor waves.

[53] Similarly, for the magnetospheric observations in Figure 13, we find that, even at distances of ~12,000 km from the surface, we still observe very similar signatures in both electrons and waves, including reflected and accelerated lunar electrons streaming outward from the Moon, narrowband electromagnetic waves, and broadband electrostatic waves. However, our location at a much larger distance from the surface allows us to see some features not obvious in previous observations. In particular, we observe clear depletions in both ions and electrons on flux tubes connected to the surface. These density depletions cannot result simply from shadowing of particles by the presence of the solid lunar obstacle, since we see depletions even in the anti-parallel (inward-going) electron fluxes. While the ambient plasma environment varies during this time period, we see nothing in the magnetic field to suggest that the spacecraft fortuitously happens to pass through a different plasma regime every time field lines connect to the surface. Instead, some process operating on the flux tubes connected to the Moon almost certainly produces the density depletions. We speculate that a wave-particle interaction scatters particles out of these flux tubes, with charge separation electric fields coupling the electrons and ions, but we leave any firm conclusion to future investigators.

[54] The ARTEMIS observations make it abundantly clear that the presence of the Moon introduces significant perturbations to plasma on connected field lines, even at quite large distances from the lunar surface. We find it fascinating to speculate on how far these perturbations extend, and how they may change the plasma processes occurring on and near these connected field lines. More detailed statistical studies utilizing the huge volume of ARTEMIS data currently accumulating (more than one periapsis pass per day, between two probes) will be needed to untangle all of the phenomena in this interesting region of space.

[55] **Acknowledgments.** We thank NASA's Lunar Science Institute for supporting this work, and acknowledge NASA contract NAS5-02099 for supporting THEMIS/ARTEMIS. FGM was supported by DLR contract 50 OC 0302. Financial support for the work of the FGM Lead Investigator Team at the Technical University of Braunschweig by the German Ministerium für Wirtschaft und Technologie and the Deutsches Zentrum für Luft- und Raumfahrt under grant 50OC1001 is acknowledged.

[56] Philippa Browning thanks the reviewers for their assistance in evaluating this paper.

References

Anderson, K. A., R. P. Lin, R. E. McGuire, and J. E. McCoy (1975), Measurement of lunar and planetary magnetic fields by reflection of low energy electrons, *Space Sci. Instrum.*, *1*, 439–470.

Angelopoulos, V. (2012), The ARTEMIS mission, *Space Sci. Rev.*, doi:10.1007/s11214-010-9687-2, in press.

Auster, H. U., et al. (2008), The THEMIS fluxgate magnetometer, *Space Sci. Rev.*, *141*, 235–264, doi:10.1007/s11214-008-9365-9.

Bale, S. D., C. J. Owen, J.-L. Bougeret, K. Goetz, P. J. Kellogg, R. P. Lin, R. Manning, and S. J. Monson (1997), Evidence of currents and unstable particle distributions in an extended region around the lunar wake, *Geophys. Res. Lett.*, *24*, 1427–1430, doi:10.1029/97GL01193.

Bale, S. D., M. J. Reiner, J.-L. Bougeret, M. L. Kaiser, S. Krucker, D. E. Larson, and R. P. Lin (1999), The source region of an interplanetary type II radio burst, *Geophys. Res. Lett.*, *26*(11), 1573–1576, doi:10.1029/1999GL900293.

Bonnell, J. W., F. S. Mozer, G. T. Delory, A. J. Hull, R. E. Ergun, C. M. Cully, V. Angelopoulos, and P. R. Harvey (2008), The electric field instrument (EFI) for THEMIS, *Space Sci. Rev.*, *141*, 303–341, doi:10.1007/s11214-008-9469-2.

Bortnik, J., J. W. Cutler, C. Dunson, and T. E. Bleier (2007), An automatic wave detection algorithm applied to Pc1 pulsations, *J. Geophys. Res.*, *112*, A04204, doi:10.1029/2006JA011900.

Davidson, R. C., and J. M. Ogden (1975), Electromagnetic ion cyclotron instability driven by ion energy anisotropy in high-beta plasmas, *Phys. Fluids*, *18*, 1045–1050, doi:10.1063/1.861253.

deHoffman, F., and E. Teller (1950), Magnetohydrodynamic shocks, *Phys. Rev.*, *80*, 692–703, doi:10.1103/PhysRev.80.692.

Farrell, W. M., R. J. Fitzenreiter, C. J. Owen, J. B. Byrnes, R. P. Lepping, K. W. Ogilvie, and F. Neubauer (1996), Upstream ULF waves and energetic electrons associated with the lunar wake: Detection of precursor activity, *Geophys. Res. Lett.*, *23*, 1271–1274, doi:10.1029/96GL01355.

Fitzenreiter, R. J., J. D. Scudder, and A. J. Klimas (1990), Three-dimensional analytical model for the spatial variation of the foreshock electron distribution function: Systematics and comparisons with ISEE observations, *J. Geophys. Res.*, *95*, 4155–4173, doi:10.1029/JA095iA04p04155.

Fitzenreiter, R. J., A. F. Vinas, A. J. Klimas, R. P. Lepping, M. L. Kaiser, and T. G. Onsager (1996), Wind observations of the electron foreshock, *Geophys. Res. Lett.*, *23*, 1235–1238, doi:10.1029/96GL00826.

Gary, S. P. (1987), The electron/electron acoustic instability, *Phys. Fluids*, *30*, 2745–2749, doi:10.1063/1.866040.

Glassmeier, K.-H., and F. M. Neubauer (1993), Low-frequency electromagnetic plasma waves at comet P/Grigg-Skjellerup: Overview and spectral characteristics, *J. Geophys. Res.*, *98*, 20,921–20,935, doi:10.1029/93JA02583.

Halekas, J. S., D. L. Mitchell, R. P. Lin, S. Frey, L. L. Hood, M. H. Acuña, and A. B. Binder (2001), Mapping of crustal magnetic anomalies on the lunar near side by the Lunar Prospector electron reflectometer, *J. Geophys. Res.*, *106*, 27,841–27,852, doi:10.1029/2000JE001380.

Halekas, J. S., R. P. Lin, and D. L. Mitchell (2005), Large negative lunar surface potentials in sunlight and shadow, *Geophys. Res. Lett.*, *32*, L09102, doi:10.1029/2005GL022627.

Halekas, J. S., D. A. Brain, D. L. Mitchell, and R. P. Lin (2006), Whistler waves observed near lunar crustal magnetic sources, *Geophys. Res. Lett.*, *33*, L22104, doi:10.1029/2006GL027684.

Halekas, J. S., D. A. Brain, R. P. Lin, and D. L. Mitchell (2008a), Solar wind interaction with lunar crustal magnetic anomalies, *Adv. Space Res.*, *41*, 1319–1324, doi:10.1016/j.asr.2007.04.003.

Halekas, J. S., G. T. Delory, R. P. Lin, T. J. Stubbs, and W. M. Farrell (2008b), Lunar Prospector observations of the electrostatic potential of the lunar surface and its response to incident currents, *J. Geophys. Res.*, *113*, A09102, doi:10.1029/2008JA013194.

Halekas, J. S., G. T. Delory, W. M. Farrell, V. Angelopoulos, J. P. McFadden, J. W. Bonnell, M. O. Fillingim, and F. Plaschke (2011a), Remote measurements of lunar surface charging from ARTEMIS: Evidence for non-monotonic sheath potentials above the dayside surface, *J. Geophys. Res.*, *116*, A07103, doi:10.1029/2011JA016542.

Halekas, J. S., Y. Saito, G. T. Delory, and W. M. Farrell (2011b), New views of the lunar plasma environment, *Planet. Space Sci.*, *59*, 1681–1694, doi:10.1016/j.pss.2010.08.011.

Halekas, J. S., A. Poppe, G. T. Delory, W. M. Farrell, and M. Horányi (2012), Solar wind electron interaction with the dayside lunar surface and crustal magnetic fields: Evidence for precursor effects, *Earth Planets Space*, *64*, 73–82.

Kennell, C. F., and H. E. Petschek (1966), Limit on stably trapped particle fluxes, *J. Geophys. Res.*, *71*, 1–28.

Li, W., J. Bortnik, R. M. Thorne, Y. Nishimura, V. Angelopoulos, and L. Chen (2011), Modulation of whistler mode chorus waves: 2. Role of density variations, *J. Geophys. Res.*, *116*, A06206, doi:10.1029/2010JA016313.

Lin, R. P., D. L. Mitchell, D. W. Curtis, K. A. Anderson, C. W. Carlson, J. McFadden, M. H. Acuña, L. L. Hood, and A. Binder (1998), Lunar

surface magnetic fields and their interaction with the solar wind: Results from Lunar Prospector, *Science*, *281*, 1480–1484, doi:10.1126/science.281.5382.1480.

Lue, C., Y. Futaana, S. Barabash, M. Wieser, M. Holmstrom, A. Bhardwaj, M. B. Dhanya, and P. Wurz (2011), Strong influence of lunar crustal fields on the solar wind flow, *Geophys. Res. Lett.*, *38*, L03202, doi:10.1029/2010GL046215.

Mazelle, C., J. B. Cao, G. Belmont, F. M. Neubauer, and A. J. Coates (1997), Compressive character of low frequency waves driven by newborn ions at comet Grigg-Skjellerup, *Adv. Space Res.*, *20*, 267–270, doi:10.1016/S0273-1177(97)00544-9.

McComas, D. J., et al. (2009), Lunar backscatter and neutralization of the solar wind: First observations of neutral atoms from the Moon, *Geophys. Res. Lett.*, *36*, L12104, doi:10.1029/2009GL038794.

McFadden, J. P., et al. (1998), Electron modulation and ion cyclotron waves observed by FAST, *Geophys. Res. Lett.*, *25*, 2045–2048, doi:10.1029/98GL00855.

McFadden, J. P., C. W. Carlson, D. Larson, M. Ludlam, R. Abiad, B. Elliott, P. Turin, M. Marckwordt, and V. Angelopoulos (2008), The THEMIS ESA plasma instrument and in-flight calibration, *Space Sci. Rev.*, *141*, 277–302, doi:10.1007/s11214-008-9440-2.

Means, J. D. (1972), Use of the three-dimensional covariance matrix in analyzing the polarization properties of plane waves, *J. Geophys. Res.*, *77*, 5551–5559, doi:10.1029/JA077i028p05551.

Mitchell, D. L., J. S. Halekas, R. P. Lin, S. Frey, L. L. Hood, M. H. Acuna, and A. Binder (2008), Global mapping of lunar crustal magnetic fields by Lunar Prospector, *Icarus*, *194*, 401–409, doi:10.1016/j.icarus.2007.10.027.

Nakagawa, T., Y. Takahashi, and M. Iizima (2003), GEOTAIL observation of upstream ULF waves associated with the lunar wake, *Earth Planets Space*, *55*, 569–580.

Nakagawa, T., F. Takahashi, H. Tsunakawa, H. Shibuya, H. Shimizu, and M. Matsushima (2009), Non-monochromatic whistler waves detected by Kaguya on the dayside surface of the moon, *Earth Planets Space*, *63*, 37–46.

Neufeld, J., and H. Wright (1964), Generation of whistler waves by helical electron beams, *Nature*, *203*, 288–289, doi:10.1038/203288a0.

Newman, D. L., R. M. Winglee, and M. V. Goldman (1988), Theory and simulation of electromagnetic beam modes and whistlers, *Phys. Fluids*, *31*, 1515–1531, doi:10.1063/1.866691.

Orlowski, D. S., G. K. Crawford, and C. T. Russell (1990), Upstream waves at Mercury, Venus and Earth: Comparison of the properties of one Hertz waves, *Geophys. Res. Lett.*, *17*, 2293–2296, doi:10.1029/GL017i013p02293.

Poppe, A., and M. Horányi (2010), Simulations of the photoelectron sheath and dust levitation on the lunar surface, *J. Geophys. Res.*, *115*, A08106, doi:10.1029/2010JA015286.

Poppe, A., J. S. Halekas, and M. Horányi (2011), Negative potentials above the day-side lunar surface in the terrestrial plasma sheet: Evidence of non-monotonic potentials, *Geophys. Res. Lett.*, *38*, L02103, doi:10.1029/2010GL046119.

Poppe, A., J. S. Halekas, G. T. Delory, W. M. Farrell, V. Angelopoulos, J. P. McFadden, J. W. Bonnell, and R. E. Ergun (2012), A comparison of ARTEMIS observations and particle-in-cell modeling of the lunar photoelectron sheath in the terrestrial magnetotail, *Geophys. Res. Lett.*, *39*, L01102, doi:10.1029/2011GL050321.

Roux, A., O. le Contel, C. Coillot, A. Bouabdellah, B. de la Porte, D. Alison, S. Ruocco, and M. C. Vassal (2008), The search coil magnetometer for THEMIS, *Space Sci. Rev.*, *141*, 265–275, doi:10.1007/s11214-008-9455-8.

Saito, Y., et al. (2008), Solar wind proton reflection at the lunar surface: Low energy ion measurements by MAP-PACE onboard SELENE (KAGUYA), *Geophys. Res. Lett.*, *35*, L24205, doi:10.1029/2008GL036077.

Saito, Y., M. N. Nishino, M. Fujimoto, T. Yamamoto, S. Yokota, H. Tsunakawa, H. Shibuya, M. Matsushima, H. Shimizu, and F. Takahashi (2012), Simultaneous observation of the electron acceleration and ion deceleration over lunar magnetic anomalies, *Earth Planets Space*, *64*, 83–92.

Santolík, O., D. A. Gurnett, G. H. Jones, P. Schippers, F. J. Crary, J. S. Leisner, G. B. Hospodarsky, W. S. Kurth, C. T. Russell, and M. K. Dougherty (2011), Intense plasma wave emissions associated with Saturn's moon Rhea, *Geophys. Res. Lett.*, *38*, L19204, doi:10.1029/2011GL049219.

Sauer, K., E. Dubinin, M. Dunlop, K. Baumgartel, and V. Tarasov (1999), Low-frequency electromagnetic waves near and below the proton cyclotron frequency at the AMPTE Ba release: Relevance to comets and Mars, *J. Geophys. Res.*, *104*, 6763–6771, doi:10.1029/1998JA900143.

Stern, S. A. (1999), The lunar atmosphere: History, status, current problems, and context, *Rev. Geophys.*, *37*(4), 453–491, doi:10.1029/1999RG900005.

Stix, T. H. (1962), *The Theory of Plasma Waves*, McGraw-Hill, New York.

Tanaka, T., et al. (2009), First in situ observation of the Moon-originating ions in the Earth's Magnetosphere by MAP-PACE on SELENE (KAGUYA), *Geophys. Res. Lett.*, *36*, L22106, doi:10.1029/2009GL040682.

Temerin, M., and R. L. Lysak (1984), Electromagnetic ion cyclotron mode (ELF) waves generated by auroral electron precipitation, *J. Geophys. Res.*, *89*, 2849–2859, doi:10.1029/JA089iA05p02849.

Temerin, M., J. McFadden, M. Boehm, and C. W. Carlson (1986), Production of flickering aurora and field-aligned electron flux by electromagnetic ion cyclotron waves, *J. Geophys. Res.*, *91*, 5769–5792, doi:10.1029/JA091iA05p05769.

Thorne, R. M., and R. B. Horne (1996), Whistler absorption and electron heating near the plasmapause, *J. Geophys. Res.*, *101*, 4917–4928, doi:10.1029/95JA03671.

Tsugawa, Y., N. Herada, Y. Katoh, T. Ono, H. Tsunakawa, F. Takahashi, H. Shibuya, and M. Matsushima (2011), Statistical analysis of monochromatic whistler waves near the Moon detected by Kaguya, *Ann. Geophys.*, *29*, 889–893, doi:10.5194/angeo-29-889-2011.

Tsurutani, B. T., D. E. Page, E. J. Smith, B. E. Goldstein, A. L. Brinca, R. M. Thorne, H. Matsumoto, I. G. Richardson, and T. R. Sanderson (1989), Low-frequency plasma waves and ion pitch angle scattering at large distances ($>3.5 \times 10^5$ km) from Giacobini-Zinner: Interplanetary magnetic field α dependence, *J. Geophys. Res.*, *94*, 18–28, doi:10.1029/JA094iA01p00018.

Wieser, M., S. Barabash, Y. Futaana, M. Holmstrom, A. Bhardwaj, R. Sridharan, M. B. Dhanya, P. Wurz, A. Schaufelberger, and K. Asamura (2009), Extremely high reflection of solar wind protons as neutral hydrogen atoms from regolith in space, *Planet. Space Sci.*, *57*, 2132–2134, doi:10.1016/j.pss.2009.09.012.

Winske, D., and N. Omidi (1992), Electromagnetic ion/ion cyclotron instability: Theory and simulations, *J. Geophys. Res.*, *97*, 14,779–14,799, doi:10.1029/92JA00902.

Wu, C. S., D. Dillenburg, L. F. Ziebell, and H. P. Freund (1983), Excitation of whistler waves by reflected auroral electrons, *Planet. Space Sci.*, *31*, 499–507, doi:10.1016/0032-0633(83)90041-7.

Yokota, S., et al. (2009), First direct detection of ions originating from the Moon by MAP-PACE IMA onboard SELENE (KAGUYA), *Geophys. Res. Lett.*, *36*, L11201, doi:10.1029/2009GL038185.